ELECTRON BEAM ANALYSIS OF THE PROPERTIES OF MOLECULAR NITROGEN AND NITRIC OXIDE IN THE AFFDL 2-FOOT ELECTROGASDYNAMICS FACILITY

S. L. Petrie, et al

Ohio State University

Prepared for:

Air Force Flight Dynamics Laboratory

February 1974

NOTICE

When Government drawings, specifications, or other data are used for any purpose other than in connection with a definitely related Government procurement operation, the United States Government thereby incurs no responsibility nor any obligation whatsoever; and the fact that the government may have formulated, furnished, or in any way supplied the said drawings, specifications, or other data, is not to be regarded by implication or otherwise as in any manner licensing the holder or any other person or corporation, or conveying any rights or permission to manufacture, use, or sell any patented invention that may in any way be related thereto.

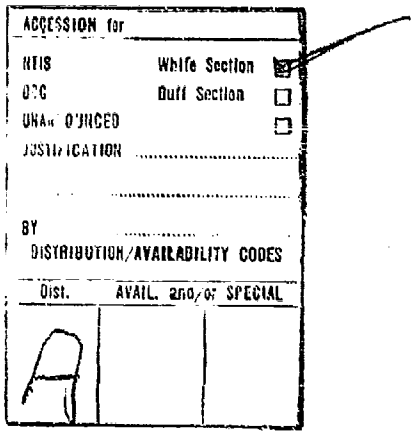

Copies of this report should not be returned unless return is required by security considerations, contractual obligations, or notice on a specific document.

AIR FORCE/56780/26 April 1974 — 150

UNCLASSIFIED

SECURITY CLASSIFICATION OF THIS PAGE (When Data Entered)

REPORT DOCUMENTATION PAGE

READ INSTRUCTIONS BEFORE COMPLETING FORM

1. REPORT NUMBER

2. GOVT ACCESSION NO.

3. RECIPIENT'S CATALOG NUMBER
AD-779087

4. TITLE (and Subtitle)
ELECTRON BEAM ANALYSIS OF THE PROPERTIES OF MOLECULAR NITROGEN AND NITRIC OXIDE IN THE AFFDL 2-FOOT ELECTROGASDYNAMICS FACILITY ✓

5. TYPE OF REPORT & PERIOD COVERED
Final
1 Dec 71 - 22 Aug 73

6. PERFORMING ORG. REPORT NUMBER

7. AUTHOR(s)
S. L. Petrie
J. J. Komar

8. CONTRACT OR GRANT NUMBER(s)
F33615-72-C-1023 NEW

9. PERFORMING ORGANIZATION NAME AND ADDRESS
The Ohio State University Research Foundation ✓
1314 Kinnear Road
Columbus, Ohio 43212

10. PROGRAM ELEMENT, PROJECT, TASK AREA & WORK UNIT NUMBERS
Project Number 1426

11. CONTROLLING OFFICE NAME AND ADDRESS
Air Force Flight Dynamics Laboratory (AFSC)
United States Air Force
Wright-Patterson AFB, Ohio 45433

12. REPORT DATE
February 1974

13. NUMBER OF PAGES
66

14. MONITORING AGENCY NAME & ADDRESS(If different from Controlling Office)

15. SECURITY CLASS. (of this report)
UNCLASSIFIED

15a. DECLASSIFICATION/DOWNGRADING SCHEDULE

16. DISTRIBUTION STATEMENT (of this Report)

Approved for public release; distribution unlimited.

17. DISTRIBUTION STATEMENT (of the abstract entered in Block 20, if different from Report)

18. SUPPLEMENTARY NOTES

19. KEY WORDS (Continue on reverse side if necessary and identify by block number)
Electron beam instrumentation; Arc-heated wind tunnel; Electrogasdynamic Facility; Molecular nitrogen; Nitric oxide; Vibrational temperature measurement; Number density measurement; Inviscid flow analysis

20. ABSTRACT (Continue on reverse side if necessary and identify by block number)

The electron beam fluorescence technique was used to measure the vibrational temperature and number density of molecular nitrogen and nitric oxide at the exit of the 7-inch conical nozzle of the Air Force Flight Dynamics Laboratory 2-Foot Electrogasdynamics Facility. In addition, the vibrational temperature and species concentration of nitric oxide were measured at the exit of the 19-inch conical nozzle. Tests were conducted at reservoir pressures of 250, 350, and 500 psia, with reservoir enthalpies varying from 2127 to 5931 BTU/lb. Theoretical results assuming finite-rate chemical

DD FORM 1 JAN 73 1473 EDITION OF 1 NOV 65 IS OBSOLETE

UNCLASSIFIED

SECURITY CLASSIFICATION OF THIS PAGE (When Data Entered)

nonequilibrium were compared with the experimental data. For the 7-inch nozzle tests, poor agreement between the measured and predicted nitrogen concentrations was obtained. The excitation-emission mechanisms for electron beam excitation of the NO γ system in NO-air and NO-nitrogen mixtures were investigated and it is shown that the excitation is dominated by secondary electrons resulting from beam-induced ionization of molecular nitrogen. Application of the electron beam technique to the measurement of nitric oxide number densities showed that the nonequilibrium theory over-predicts the amount of nitric oxide present in the expansion process. Reasons for the discrepancies between the theoretical and experimental results were examined.

*U.S.Government Printing Office: 1974 — 758-433/533

AFFDL-TR-74-8

ELECTRON BEAM ANALYSIS OF THE PROPERTIES OF MOLECULAR NITROGEN AND NITRIC OXIDE IN THE AFFDL 2-FOOT ELECTROGASDYNAMICS FACILITY

S. L. Petrie

J. J. Komar

FOREWORD

This technical report was prepared by S. L. Petrie and J. J. Komar of the Aeronautical and Astronautical Research Laboratory of The Ohio State University Research Foundation on Contract F33615-72-C-1023 (RF 3361-A1). The research reported here was performed on Task 142601. H. Lee of the Air Force Flight Dynamics Laboratory, Wright-Patterson Air Force Base, Ohio was the project engineer for the contract and for the facility tests.

This report covers work conducted from 1 December 1971 to 22 August 1973.

The manuscript was released by the authors in August, 1973, for publication as a technical report.

This technical report has been reviewed and is approved.

Philip P. Antonatos
Chief, Flight Mechanics Division
Air Force Flight Dynamics Laboratory

ABSTRACT

The electron beam fluorescence technique was used to measure the vibrational temperature and number density of molecular nitrogen and nitric oxide at the exit of the 7-inch conical nozzle of the Air Force Flight Dynamics Laboratory 2-Foot Electrogasdynamics Facility. In addition, the vibrational temperature and species concentration of nitric oxide were measured at the exit of the 19-inch conical nozzle. Tests were conducted at reservoir pressures of 250, 350, and 500 psia, with reservoir enthalpies varying from 2127 to 5931 Btu/lb. Theoretical results assuming finite-rate chemical nonequilibrium were compared with the experimental data. For the 7-inch nozzle tests, poor agreement between the measured and predicted nitrogen concentrations was obtained. The excitation-emission mechanisms for electron beam excitation of the NO γ system in NO-air and NO-nitrogen mixtures were investigated and it is shown that the excitation is dominated by secondary electrons resulting from beam-induced ionization of molecular nitrogen. Application of the electron beam technique to the measurement of nitric oxide number densities showed that the nonequilibrium theory over-predicts the amount of nitric oxide present in the expansion process. Reasons for the discrepancies between the theoretical and experimental results were examined.

TABLE OF CONTENTS

Section		Page
I	INTRODUCTION	1
II	ELECTRON BEAM THEORY	2
	A. GENERAL CONSIDERATIONS	2
	B. VIBRATIONAL TEMPERATURE MEASUREMENT	3
	C. NUMBER DENSITY MEASUREMENT	4
III	CALIBRATION EXPERIMENTS	10
	A. GENERAL APPROACH	10
	B. ELECTRON BEAM GENERATOR	10
	C. INSTRUMENTATION	10
	D. CALIBRATION RESULTS	14
IV	APPARATUS AND PROCEDURES	21
	A. WIND TUNNEL SYSTEM AND INSTRUMENTATION	21
	B. ELECTRON BEAM SYSTEM	22
	C. TEST PROCEDURES	24
	D. DATA REDUCTION TECHNIQUES	24
V	RESULTS AND DISCUSSIONS	29
	A. THEORETICAL ANALYSES	29
	B. NOMINAL RUN CONDITIONS	29
	C. PROBE DATA	29
	D. VIBRATIONAL TEMPERATURES	35
	E. NUMBER DENSITIES	43
VI	CONCLUSIONS	52
	A. ELECTRON BEAM TECHNIQUES	52
	B. THEORETICAL-EXPERIMENTAL COMPARISONS	52
REFERENCES		54

LIST OF TABLES

Table		Page
I	PROBE LOCATIONS IN INCHES DOWNSTREAM OF NOZZLE EXIT	21
II	QUENCHING CONSTANTS	27
III	NOMINAL RESERVOIR CONDITION SUMMARY	30

LIST OF ILLUSTRATIONS

Figure		Page
1	Ratio of Intensities for the (1,5) and (0,2) Bands of the NO γ and (0,1) and (1,2) Bands of the N_2^+ Systems	5
2	$S(T_V)/S(300\ K)$ for $(0,v'')$ and $(1,v'')$ Bands of the N_2^+ and NO γ Systems	9
3	Electron Beam Generator-Gap Lens Schematic	11
4	Electron Beam Generator Schematic	12
5	Calibration Instrumentation Schematic	13
6	Intensity of NO γ (0,2) Band in Various Gas Mixtures	15
7	Intensity of NO γ (1,5) Band in Various Gas Mixtures	16
8	Spectral Scan of NO γ System in 67% NO, 33% Air	18
9	I/I_0' for NO γ (0,2) and (1,5) Bands	20
10	Instrumentation Schematic	23
11	Typical Run Record of Spectral Scans	25
12	Test Chamber Installation in the 2-Foot EGF	27
13	Pitot Pressure Surveys at Run Condition 2; 19-Inch Nozzle; p_0 = 350 psia	30
14	Pitot Pressure Surveys at Run Condition 3; 19-Inch Nozzle; p_0 = 500 psia	31

LIST OF ILLUSTRATIONS - (Continued)

Figure		Page
15	Pitot Pressure Surveys at Run Condition 1; 7-Inch Nozzle; p_0 = 250 psia	32
16	Pitot Pressure Surveys at Run Condition 2; 7-Inch Nozzle; p_0 = 350 psia	33
17	Pitot Pressure Surveys at Run Condition 3; 7-Inch Nozzle; p_0 = 500 psia	34
18	Pitot Pressure Surveys at Various Axial Stations - Run Condition 1, 7-Inch Nozzle	36
19	Pitot Pressure Surveys at Various Axial Stations - Run Condition 2, 7-Inch Nozzle	37
20	Pitot Pressure Surveys at Various Axial Stations - Run Condition 3, 7-Inch Nozzle	38
21	Axial Centerline Pitot Pressures; 7-Inch Nozzle	39
22	N_2 Vibrational Temperatures; 7-Inch Nozzle	40
23	NO Vibrational Temperatures; 7-Inch Nozzle	41
24	NO Vibrational Temperatures; 19-Inch Nozzle	42
25	N_2 Number Densities at Run Condition 1; 7-Inch Nozzle	44
26	N_2 Number Densities at Run Condition 3; 7-Inch Nozzle	45
27	NO Number Densities at Run Condition 2; p_0 = 350 psia; 7-Inch Nozzle	47
28	NO Number Densities at Run Condition 3; p_0 = 500 psia; 7-Inch Nozzle	48
29	NO Number Densities at Run Condition 2; p_0 = 350 psia; 19-Inch Nozzle	49
30	NO Number Densities at Run Condition 3; p_0 = 500 psia; 19-Inch Nozzle	50

LIST OF SYMBOLS

A_{ji}	spontaneous probability for j → i transition
c	speed of light
c_1	calibration constant
f_j	fraction of photons absorbed by species j in ground electronic energy state
$G(v_o)$	vibrational term value in ground electronic energy state
h	Planck's constant
H_o	stagnation enthalpy
I	photomultiplier current
I_{ji}	intensity of radiation
I'_o	photomultiplier current with no excitation by secondary electrons
J	electron beam current
k	Boltzmann's constant
m	particle mass
N	total number density
N_k	number density of species k
N'_k	quenching density of species k
N_{N_2}, $[N_2]$	N_2 number density
N_{NO}, [NO]	NO number density
p	static pressure
p'	quenching pressure
p_o	stagnation (reservoir) pressure
p_{T_2}	pitot pressure
$Q_o(v_e)$	cross section for excitation by primary electrons

$Q_{kB}(v_s)$	cross section for excitation of species k by secondary electrons
$Q_{kT}(v_e)$	total cross section for ionization of species k by primary electrons
$\dot{q}$	heat transfer rate
$q(v',v'')$	Franck-Condon factor for v' → v'' transition
$S(T_v)$	vibrational temperature correction to density
T	translational temperature
T_v	vibrational temperature
t	time
v', v'', v_o	vibrational quantum numbers
v_e	primary electron velocity
v_s	secondary electron velocity
Z_{kj}	collision frequency for collisions between species k and j
ν, ν_{ji}	wavenumber for j → i transition
λ_s	mean free path function for secondary electrons
ρ	mass density

Subscripts

c	for pre-run calibration conditions
o	for reservoir conditions
sc	for conditions in static test chamber
I	for Channel I
II	for Channel II

Superscripts

*	for properties in excited electronic energy state

I. INTRODUCTION

Arc-heated wind tunnels are generally characterized by a high degree of thermodynamic and chemical nonequilibrium within the expansion process. To predict test-section gas properties and properly interpret model data obtained with such facilities, an accurate theoretical analysis of the flow process employing finite-rate chemical and thermodynamic reactions is required. The accuracy of the analysis depends directly on the applicability of the kinetic model (i.e., the set of reactions employed) and the availability of the appropriate rate constants.

While certain wind tunnel calibration data (i.e., pitot pressure, flow velocity, stagnation point heat transfer rate) are relatively independent of the detailed thermochemical processes, other calibration factors such as the static temperature, Mach number, Reynolds number, etc., are not. Since many of the quantities which cannot be directly measured must be known to relate the wind tunnel data to equivalent flight conditions, an accurate theoretical model must be available. The accuracy of such a model can be determined if appropriate measurements can be made which will allow comparison of the theoretical results with experimental data.

The chemical species of interest for much of the operating ranges of typical arc-heated wind tunnels consist of: N_2, N, O_2, O, NO, NO^+, and e^-. While N_2, O, and O_2 make up at least 95% of the gas mixture, nitric oxide can be extremely important in determining the gas composition. The nitric oxide shuffle reactions, $N_2 + O \rightarrow NO + N$, $N + O_2 \rightarrow NO + O$, and $N_2 + O_2 \rightarrow NO + NO$, are bimolecular and hence, are extremely rapid. In certain operating ranges, these shuffle reactions control the rate of oxygen recombination in the nozzle expansion process, and thereby heavily influence the resulting gas properties at the nozzle exit. Hence, measurement of the properties of nitric oxide can be extremely useful in determining the accuracy of the shuffle reaction rates and their relative effects on the results of the theoretical predictions.

A series of experiments has been performed in the AFFDL 2-Foot Electrogasdynamic Facility (EGF) in which the electron beam diagnostic technique has been applied for the measurement of certain gas properties. In Ref. 1, the technique was applied for the measurement of the vibrational temperature, rotational temperature, and number density of molecular nitrogen. In Ref. 2, the species concentrations of molecular and atomic oxygen, and the vibrational temperature of molecular oxygen were determined. Application of the electron beam diagnostic technique to the determination of the properties of nitric oxide were investigated by Petrie and Komar.[3] The calibration experiments of Ref. 3 have been extended and the diagnostic techniques have been applied for measuring the properties of nitric oxide in the 2-foot EGF operating at nominal flow Mach numbers of 8 and 10. In addition, the vibrational temperature and number density of molecular nitrogen have been measured at a flow Mach number of 8 to extend the lower density measurements of Ref. 1.

As in Refs. 1 and 2, the electron beam data are compared with usual facility operating parameters and nozzle exit pitot pressures to determine the properties of the test gas at the measuring station. These experimental results are compared with those from the theoretical analysis to provide additional information useful for assessing the applicability of the theoretical model.

The general theory for electron-induced radiation in nitric oxide is summarized in Section II. Section III describes the experimental techniques used, and the results of certain calibration experiments. The remaining sections describe the application of the diagnostic techniques in the 2-foot EGF.

II. ELECTRON BEAM THEORY

A. GENERAL CONSIDERATIONS

Radiation intensities sufficient for accurate determination of gas properties in an arc-heated wind tunnel can be obtained with electron beam currents near 20 mA at beam voltages from 5 to 75 kV. The beam is projected across the flow, and the interaction of electrons with gas particles produces a column of radiation which is nearly coincident with the beam of electrons. Profiles of gas properties are obtained by examining various points along the length of the beam. High-beam voltages are required to obtain good spatial resolution in the measurements; at low-beam voltages and high gas densities elastic scattering of the beam electrons is severe.

When an electron beam is passed through the flow at the nozzle exit, radiation is observed due to bombardment of most species known to exist in the flow field. The radiation resulting from excitation of molecular nitrogen and nitric oxide is of particular interest.

The predominant radiation due to excitation of molecular nitrogen is the first negative system of the ionized nitrogen molecule (N_2^+). The most intense band is the (0,0) band at 3914 Å. Much experimental work (summarized in Ref. 4) has been done with the first negative system in nitrogen and air to verify the applicability of the diagnostic technique. Details of the methods can be found in Refs. 1 and 4-7.

Electron beam excitation of nitric oxide results in observation of radiation in the γ, Ogawa, and Feast systems.[3] In air flows, the γ system is useful for vibrational temperature and number density measurements at wavelengths below approximately 3044 Å. At higher wavelengths, the γ bands are overlapped by bands from the N_2^+ systems. The Feast and Ogawa systems appear only weakly at wavelengths between 5800 and 6100 Å and relatively little is known of their structure. The uncertainties associated with these systems and their low radiation intensities makes them unsuitable now for electron beam diagnostics.

The electronic transition comprising the NO γ system is denoted by $NO(A^2\Sigma^+) \rightarrow NO(X^2\Pi)$. Emission is excited by collisions between electrons and nitric oxide molecules in the ground electronic energy state $NO(X^2\Pi)$. Detailed considerations of the excitation-emission process in pure nitric oxide are given by Petrie and Komar[3] and will not be repeated here. It should be noted, however, that the transitions are resonant. That is, the excitation and emission processes connect the same electronic states so that self-absorption of the radiation is possible. The analysis of Ref. 3 indicates that self-absorption can be neglected for nitric oxide number density-path length products at least up to 10^{19} cm^{-2}, for transitions which do not involve the ground vibrational energy level. In the studies reported here, only those bands not involving the ground vibrational energy state were used so that self-absorption effects can be neglected.

For both molecular nitrogen and nitric oxide, it is assumed that excitation occurs with no perturbation in the rotational and vibrational population distributions in the ground electronic energy state. Since the Born approximation is assumed to apply, only those transitions which are allowed by optical selection rules are considered. Hence, both the excitation and emission transitions are assumed to be governed by the Franck-Condon principle.

The rotational structure of the NO γ bands is quite complicated since the emission is a $^2\Sigma^+$-$^2\Pi$ transition. Separation of the individual rotational lines requires both high spectral resolution and very intense radiation so that an acceptable signal-to-noise ratio can be obtained. As discussed in Ref. 2, for rotational temperature measurement there is little need to resolve the rotational structure of bands other than those in the N_2^+ first negative system. The rapid equilibration of the rotational energy modes of all heavy species with the translational energy mode allows the rotational temperature of each species to be assumed equal to the translational temperature of the gas. Hence, the measurement of the rotational temperature of molecular nitrogen will suffice to describe the rotational and translational temperatures of all heavy species.

B. VIBRATIONAL TEMPERATURE MEASUREMENT

The ratios of intensities of two vibrational bands in both the N_2^+ first negative and NO γ systems are determined by assuming that the populations of the vibrational energy levels of both N_2 and NO can be described by Boltzmann distributions with vibrational temperatures which need not be equal to the translational temperature nor equal to each other. The ratio of intensities of two vibrational bands is given by

$$\frac{I_1}{I_2} = \left(\frac{\nu_1}{\nu_2}\right)^4 \frac{q_1}{q_2} \frac{\sum_{v_0} q_1(v_1', v_0)\, e^{-G(v_0)hc/kT_V}}{\sum_{v_0} q_2(v_2', v_0)\, e^{-G(v_0)hc/kT_V}} \frac{\sum_{v''} \nu_2^3 q(v_2', v_2'')}{\sum_{v''} \nu_1^3 q(v_1', v_1'')} \qquad (1)$$

where q_1 and q_2 are the Franck-Condon factors for the emission transitions, $q(v_1', v_0)$ is the Franck-Condon factor for the excitation transition from the v_0 vibrational energy level in the ground electronic state to the v_1' vibrational level in the excited electronic energy state, and $G(v_0)$ is the vibrational term value in the ground electronic energy state.

From Eq (1), the ratio of intensities of two bands in the emission is a function only of the vibrational temperature of the molecules in the ground electronic energy state. The ratios of intensities of various band combinations for both molecular nitrogen and nitric oxide are shown as functions of vibrational temperature in Figure 1. The Franck-Condon factors employed to construct Figure 1 are given in Refs. 1 and 3.

With the assumption of direct excitation, the vibrational temperatures are determined by measuring the relative intensities of the vibrational bands and consulting the curves of Figure 1. It is notable that much greater sensitivity to vibrational temperature is obtained with molecular nitrogen than it is with nitric oxide. The relatively small variation in intensity ratio with vibrational temperature for nitric oxide places severe requirements on the electro-optical system employed to make the band intensity measurements.

C. NUMBER DENSITY MEASUREMENT

It is a common practice to determine the number density by measuring the intensity of one or more vibrational bands which appear in the beam-excited emission. In order to interpret the band intensity in terms of number density, the excitation-emission mechanisms which lead to the radiation must be known. It is well known that for molecular nitrogen, the N_2^+ first negative system is excited primarily by beam electrons and that secondary electrons have a negligible effect. However, because of the low excitation energy of the NO γ upper state (5.2 eV compared to 18 eV for the $N_2^+(B^2\Sigma)$ state), secondary excitation mechanisms may be important in producing the NO γ system.

As described in Ref. 8, the rate of excitation of gas molecules to excited electronic energy states due to excitation by primary and secondary electrons can be given by

$$\frac{dN_j^*}{dt} = N_e v_e N_j Q_0(v_e) + \frac{N_e v_e N_j Q_{je}(v_s) \sum_k N_k Q_{kT}(v_e)}{\sum_k N_k Q_{ks}(v_s) + \lambda_s^2} \qquad (2)$$

where the first term accounts for excitation by primary electrons and the second term allows for excitation by secondary electrons. N_j^* denotes the number density of excited species, N_e is the electron

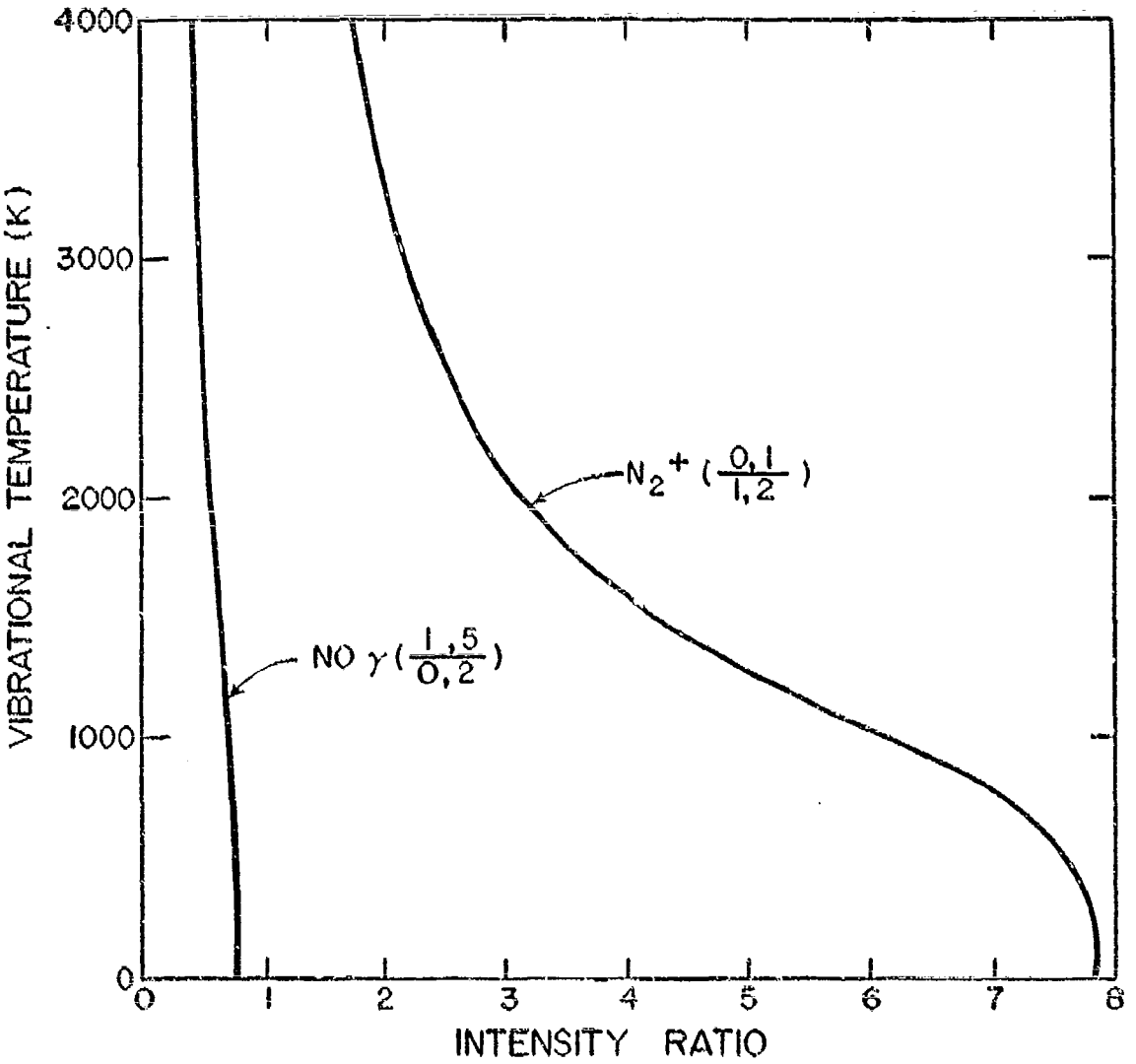

Figure 1. Ratio of Intensities for the (1,5) and (0,2) Bands of the NO γ and (0,1) and (1,2) Bands of the N_2^+ Systems

number density within the beam, v_e is the velocity of the primary electrons, N_j is the number density of the species in the ground electronic energy state, and λ_s is related to the diffusion coefficient of the secondary electrons. The quantities $Q_o(v_e)$ and $Q_{js}(v_s)$ are the cross sections for excitation of species j by primary electrons and secondary electrons and $Q_{kI}(v_e)$ and $Q_{ks}(v_s)$ are the total cross sections for ionization of species k and excitation of species k by secondary electrons.

Since the NO γ system is resonant, population of the upper electronic energy state as a result of absorption of resonant photons should be included in the analysis. In addition, excitation caused by the collision of ground state molecules with electronically excited particles can be included. The rate of excitation due to these two mechanisms is given by

$$\frac{dN_j^*}{dt} = f_j A_{ji} N_j^* + \sum_k Z_{kj} N_k^* \tag{3}$$

where f_j is the fraction of the resonant photons absorbed, A_{ji} is the transition probability for spontaneous emission, and Z_{kj} is the frequency of collisions between ground state molecules and excited particles of species k. Note that induced emission is ignored in Eq (3).

The collision frequency Z_{kj} is given in the same form as that for usual binary encounters except that the cross section for excitation is employed instead of the simple kinetic cross section. Hence,

$$Z_{kj} = 4 N_j Q_{kj} \sqrt{kT/m\bar{i}} \tag{4}$$

To allow explicit appearance of the number densities, the collision frequency is rewritten as

$$Z'_{kj} = Z_{kj}/N_j \tag{5}$$

Depopulation of the excited state is assumed to occur due to spontaneous radiative transitions and collision quenching. Hence,

$$-\frac{dN_j^*}{dt} = N_j^* \left\{ \left(A_{ji} + \sum_{k \neq i} A_{jk} \right) + \sum_k N_k Q_{kc} \right\} \tag{6}$$

where Q_{kc} is a "quenching speed" with units of cross section times speed.[8]

In the steady state, Eqs (2)-(6) give the concentration of excited particles as

$$N_j^* = \frac{1}{(A_{ji} + A)\left[1 - \frac{f_j A_{ji}}{A_{ji} + A} + \sum_k N_k/N_k'\right]} \times$$

$$\left\{ N_e v_e N_j Q_o(v_e) + \frac{N_e v_e N_j Q_s(v_s) \sum_k N_k Q_{kT}(v_e)}{\sum_k N_k Q_{ks}(v_s) + \lambda_s^2} + \sum_k Z_{kj}' N_k N_j \right\} \qquad (7)$$

where $N_k' = (A_{ji} + A)/Q_{kc}$ is considered a quenching number density[8] and $A = \sum_{k \neq j} A_{jk}$.

The intensity of the radiation is given by

$$I_{ji} = N_j^* h c \nu_{ji} A_{ji} \qquad (8)$$

where h is Planck's constant, c is the speed of light and ν_{ji} is the wavenumber of the $j \rightarrow i$ transition. The output of a photomultiplier viewing the radiation is related to the intensity by various sensitivity factors which arise because of absorption by optical components, the instrument function of the device used for spectral resolution, the photomultiplier gain, etc. These factors are combined into a single calibration constant, c_1, which also includes the multiplicative constant which relates N_e, v_e, and the electron beam cross-sectional area to the beam current, J. Hence, the ratio of photomultiplier signal-to-beam current is given by

$$\frac{I}{J} = \frac{c_1}{1 - \frac{f_j A_{ji}}{A_{ji} + A} + \sum_k N_k/N_k'} \times$$

$$\left\{ Q_o(v_e) N_j + \frac{Q_s(v_s) N_j \sum_k N_k Q_{kT}(v_e)}{\sum_k N_k Q_{ks}(v_s) + \lambda_s^2} + \sum_k \frac{Z_{kj}'}{J} N_j N_k^* \right\} \qquad (9)$$

The constant c_1 must be determined by calibrating the entire electro-optical system. This is usually done under room-temperature conditions. However, the intensity of a vibrational band depends upon the various factors of Eq (9) and the vibrational temperature. To account for the vibrational temperature effects, the photomultiplier current can be given by[1,8]

$$\frac{I}{J} = [c_1 S(T_c)]\left[\frac{S(T_v)}{S(T_c)}\right] \frac{N_j}{1 - \frac{f_j A_{ji}}{A_{ji} + A} + \sum_k N_k/N_k'} X$$

$$\left\{ Q_o(v_e) + \frac{Q_s(v_s) \sum_k N_k Q_{kT}(v_e)}{\sum_K N_k Q_{ks}(v_s) + \lambda_s^2} + \sum_k \frac{2'_{kj}}{J} N_k'' \right\} \tag{10}$$

where

$$S(T_v) = \frac{\nu_{ji}^4 q(v',v'')}{Q_v(T_v)} \frac{\sum_{v_o} q(v_o,v') \, e^{-G(v_o)hc/kT_v}}{\sum_{v''} q(v',v'') \nu^4_{v',v''}} \tag{11}$$

and $S(T_c)$ is $S(T_v = 300\ K)$. The functions $S(T_v)/S(T_c)$ for the $v' = 0$ and 1 progressions for the N_2^+ first negative and NO γ systems are given in Figure 2.

In a strict sense, the correction for vibrational temperature effects applies only to that portion of the excitation due to primary electrons (a similar form can be written for the resonant absorption term). Collisional excitation by secondary electrons and excited particles may be accompanied by perturbation in the vibrational population distribution so that Eq (11) no longer applies to the entire excitation process. In addition, preferential collision quenching of various excited vibrational energy levels may occur. These effects must be evaluated in specific applications before the excitation-emission analysis can be applied with confidence.

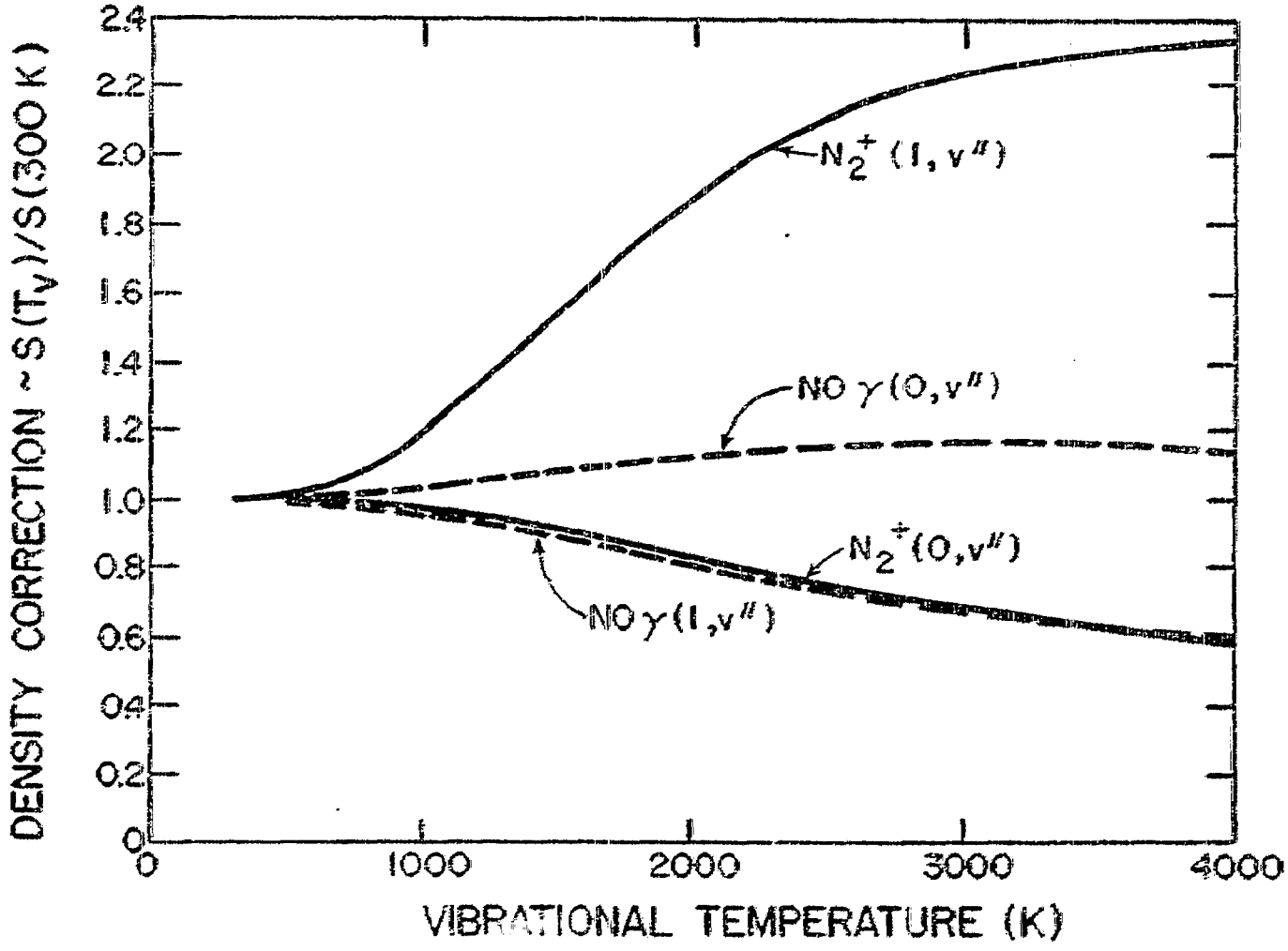

Figure 2. $S(T_v)/S(300\ K)$ for (0,v") and (1,v") Bands of the N_2^+ and NO γ Systems

III. CALIBRATION EXPERIMENTS

A. GENERAL APPROACH

A series of calibration experiments was conducted to evaluate the relative importance of the various excitation mechanisms accompanying electron excitation of nitric oxide. The variations of the radiative intensities of the (0,2) and (1,5) bands of the NO γ system were investigated over a range of gas density in pure nitric oxide, nitric oxide-air, and nitric oxide-nitrogen mixtures. The experiments extend those of Ref. 3 which were conducted only in pure nitric oxide. The results are interpreted in terms of the excitation-emission analysis of Ref. 3 and Section II.

B. ELECTRON BEAM GENERATOR

The electron beam generator used for the calibration experiments is shown schematically in Figure 3. The system differs from that described in Refs. 2 and 3 and used in the previous EGF experiments. The present electron beam generator allows accelerating potentials up to 75 kV, while the older version was limited to voltages up to about 20 kV.

The electron beam generator consists of a duoplasmatron electron source, a gap lens for beam forming, and electromagnetic beam steering and focusing systems. The lens elements are mounted inside a 6-inch standard steel tee which is connected to a 6-inch oil diffusion pump. A baffle is used between the diffusion pump and the beam chamber to reduce backstreaming of diffusion pump oil. The electrons exit from the beam chamber through a 0.03-inch-diameter, 0.30-inch-long exit channel.

The maximum acceleration potential is 75,000 V with a maximum beam current of 60 mA. To minimize defocusing of the beam as it traverses the drift tube and passes through the exit orifice, the electrons are accelerated from high potentials toward ground potential. An electrical schematic of the beam generator system is given in Figure 4.

C. INSTRUMENTATION

The main optical instrumentation system employed in the calibration studies is shown schematically in Figure 5 and is described in detail in Ref. 3. Spectral resolution was accomplished with a Jarrell-Ash 0.5-m Ebert scanning spectrometer. The grating was ruled with 30,000 lines/in. yielding a disperaion of 16 Å/mm and a maximum resolution of 0.2 Å. An EMI 6256S photomultiplier was used with the spectrometer. The photocurrents were measured and amplified with a Keithley Model 417 picoammeter. The beam current was monitored by measuring the voltage drop across the

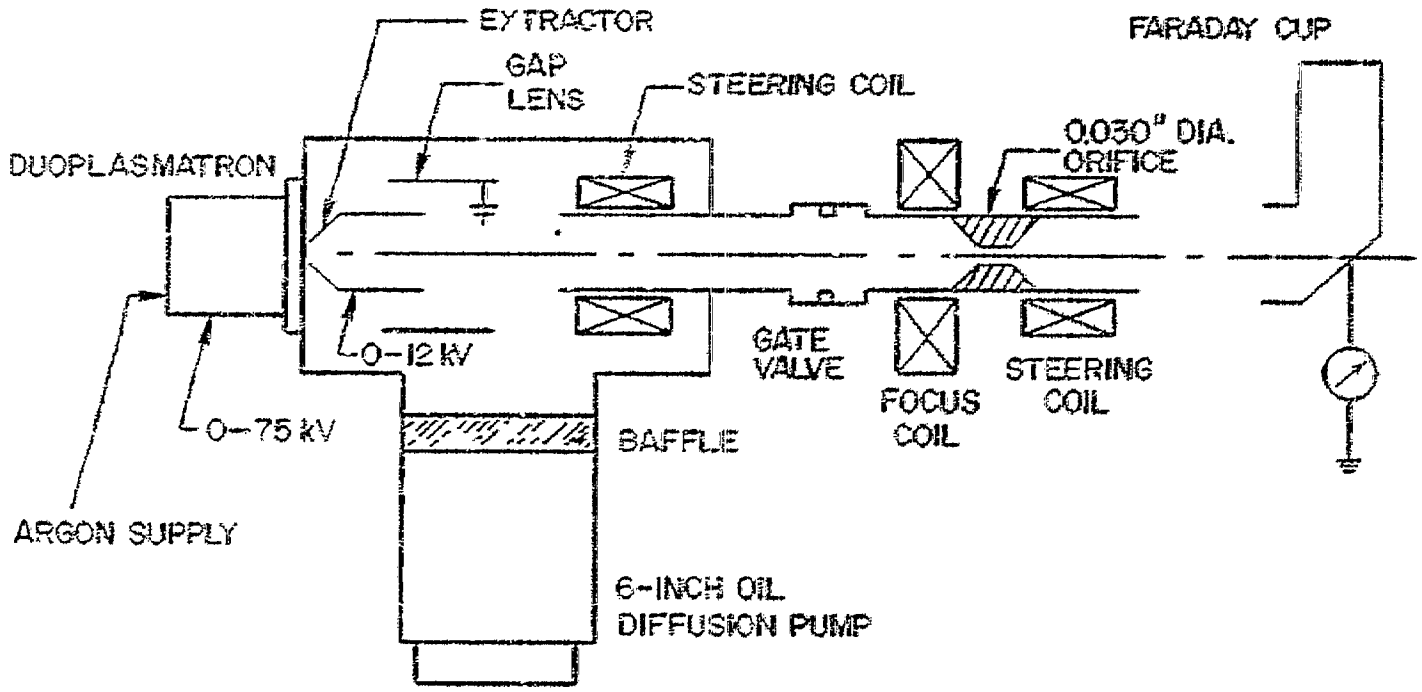

Figure 3. Electron Beam Generator-Gap Lens Schematic

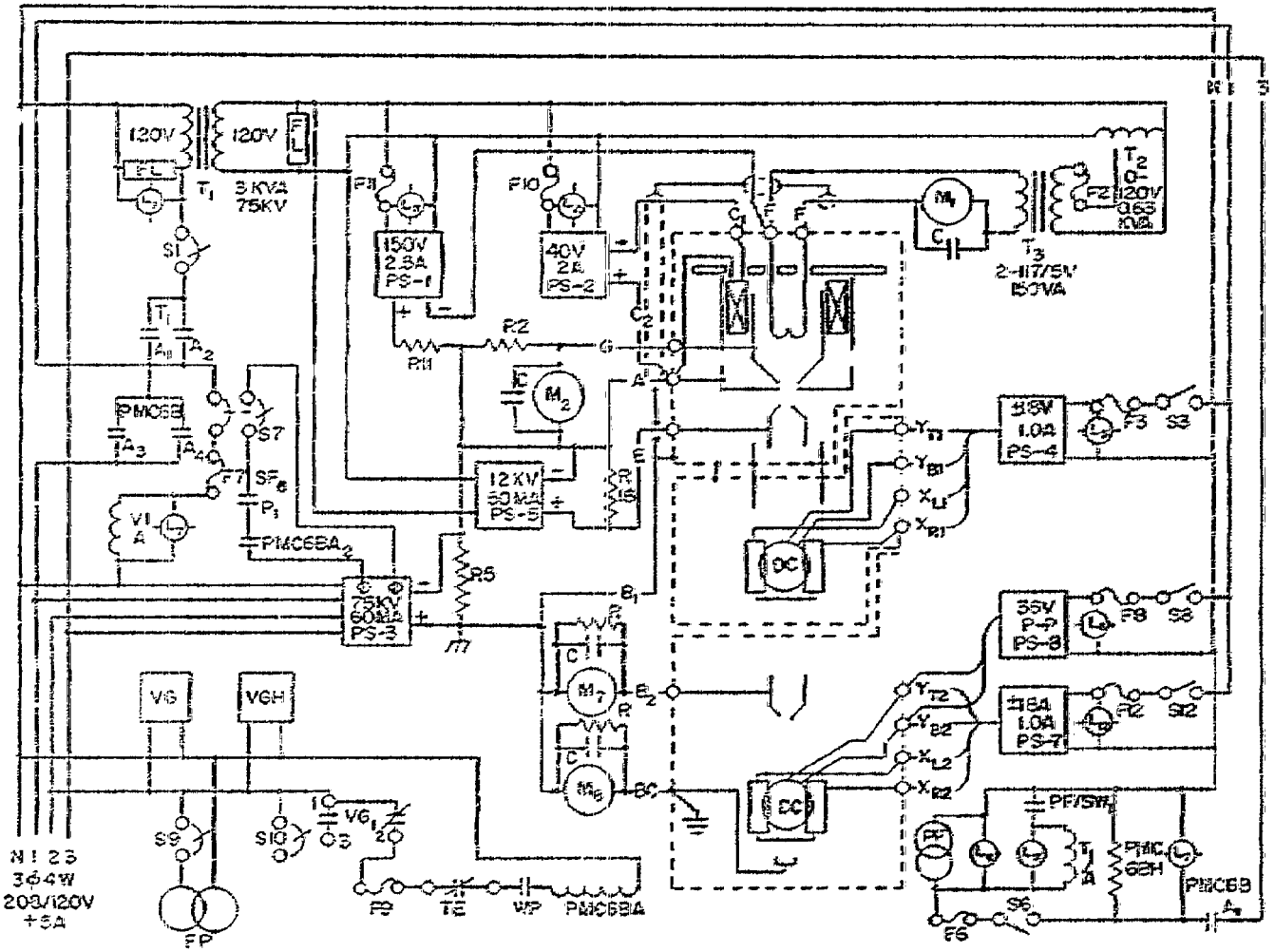

Figure 4. Electron Beam Generator Schematic

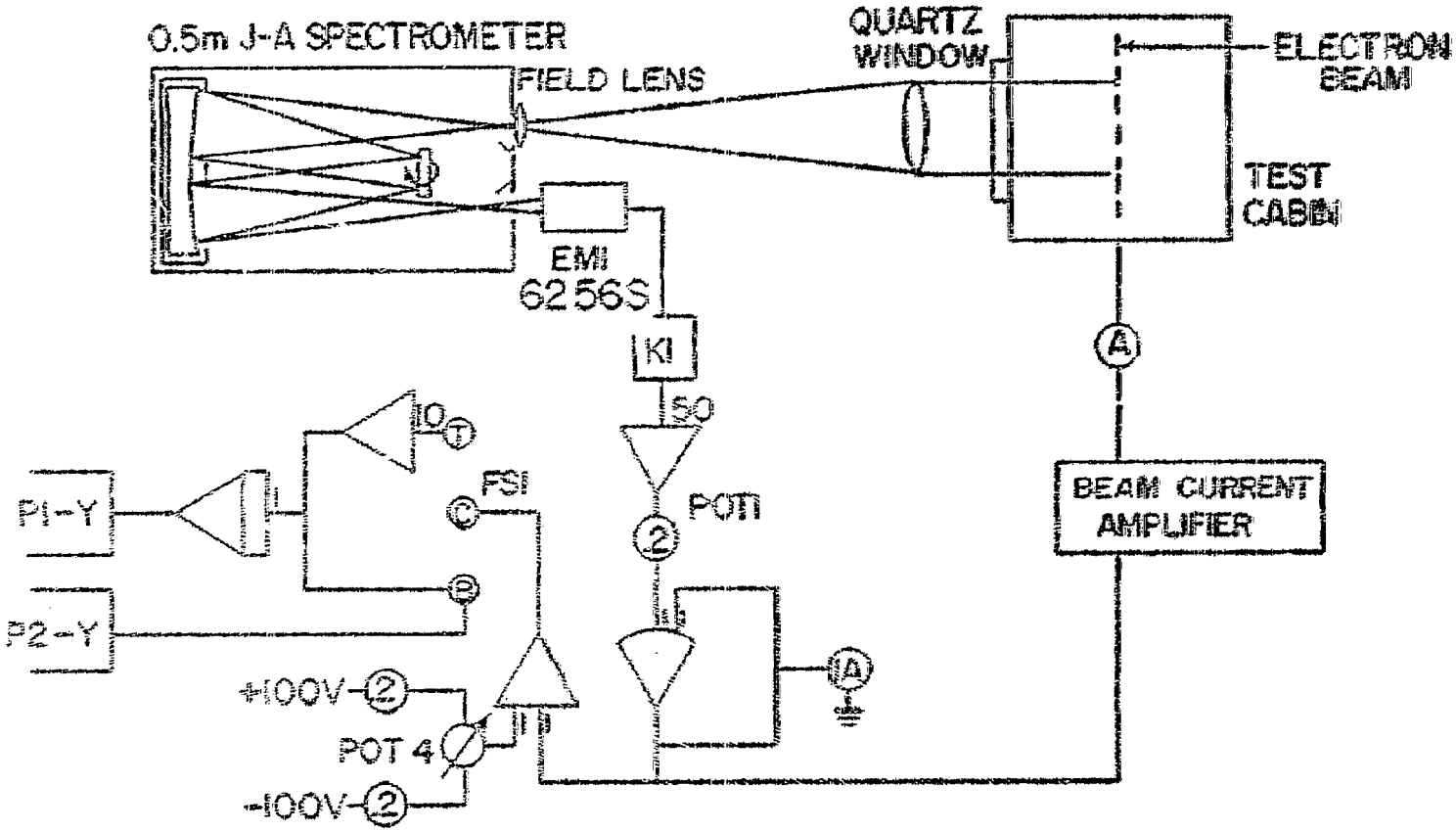

Figure 5. Calibration Instrumentation Schematic

beam current ammeter. The outputs from the picoammeter and beam current ammeter entered an on-line analog computer where the ratios of the photomultiplier and beam current signals were formed, and the results were displayed on X-Y plotters. Since the photomultiplier output varies linearly with beam current, the ratio of signals is a true measure of the relative intensity of the region of the spectrum under investigation with the spectrometer.

For the calibration experiments, the electron beam was projected into an 18-inch-diameter, 18-inch-long cadmium-plated steel test chamber. The electron beam generator was electrically isolated from the test chamber so that the entire chamber served as a Faraday cage for the measurement of beam current. The electron beam was captured in a water-cooled 90° elbow to eliminate back-scattering of low energy electrons. Previous tests have demonstrated that this configuration virtually eliminates radiation due to excitation by secondary electrons resulting from bombardment of the chamber walls by beam electrons.

Mixtures of nitric oxide-nitrogen and nitric oxide-air were supplied through two separate flow metering systems. Nitric oxide was supplied by one metering system, while either air or nitrogen was supplied by the other. The gases were mixed dynamically in the test chamber. Dynamic mixing was chosen over the simpler procedure of using pre-mixed gases to reduce the chemical reactions which occur between nitric oxide and molecular oxygen in NO-air mixtures.

The tests were conducted by evacuating the test chamber to a pressure less than 1 μm Hg and pumping on the system for at least 30 minutes. The desired flow rates of nitric oxide and the second gas were then established with the flow meters. At that time the valve between the vacuum pump and the test chamber was closed and the output of the photomultiplier divided by beam current was plotted versus the chamber pressure on an X-Y plotter. Raw photomultiplier and beam current signals were also plotted versus pressure. The rate of pressure rise was low enough to assure that all electrical components responded to the change in signals accompanying the pressure increases.

The pressure in the test chamber was measured with a variable reluctance pressure transducer. The electrical output of the transducer was sent to the analog computer where various calibration constants were applied to obtain corrected pressure. The resulting pressure was recorded on X-Y plotters.

D. CALIBRATION RESULTS

The intensities of the NO γ (0,2) and (1,5) bands are plotted versus NO partial pressure in Figures 6 and 7. It is clear that the band intensities do not correlate with the NO partial pressure, which would indicate the presence of excitation mechanisms in addition to direct excitation by beam electrons.

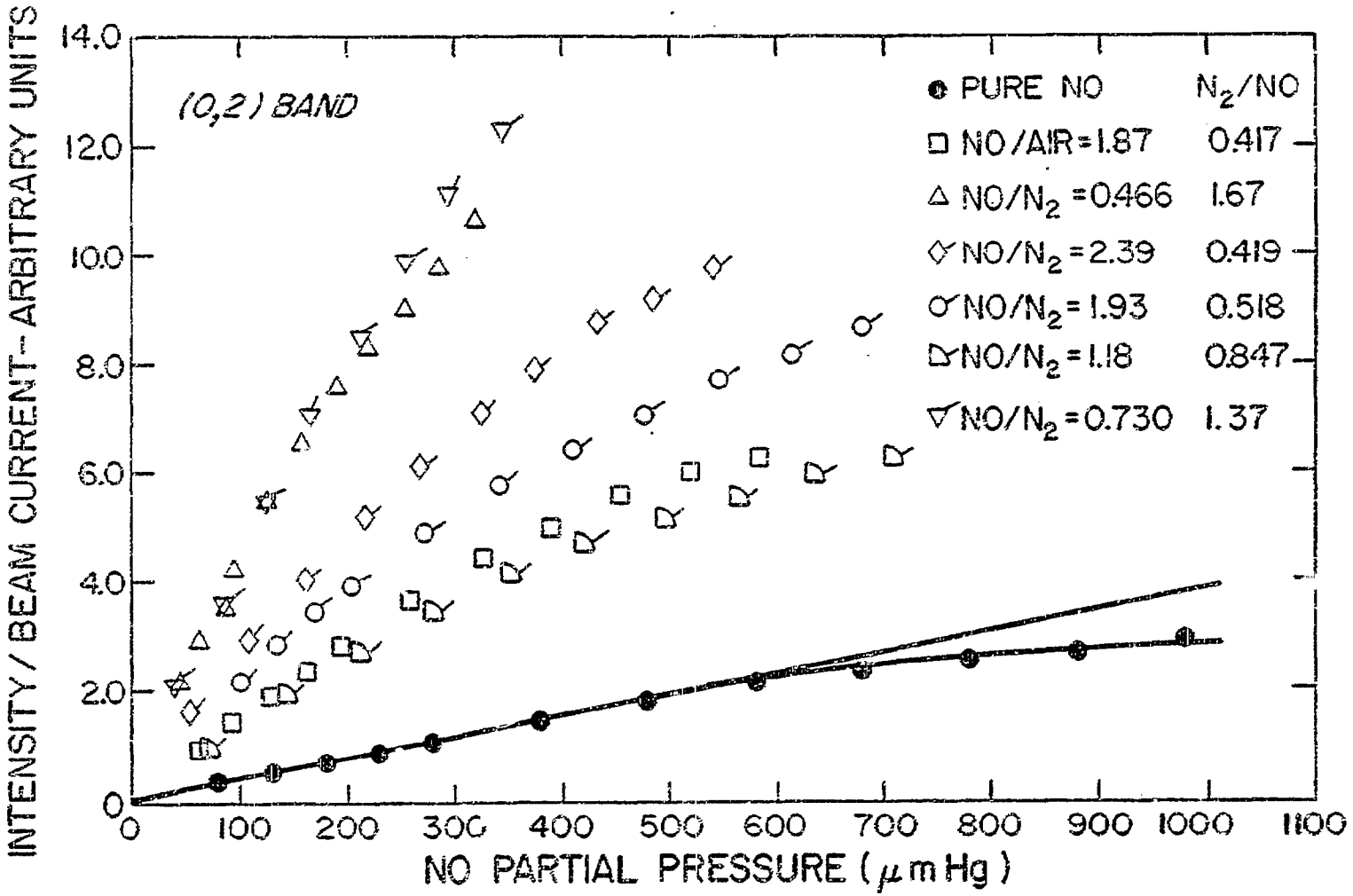

Figure 6. Intensity of NO γ (0,2) Band in Various Gas Mixtures

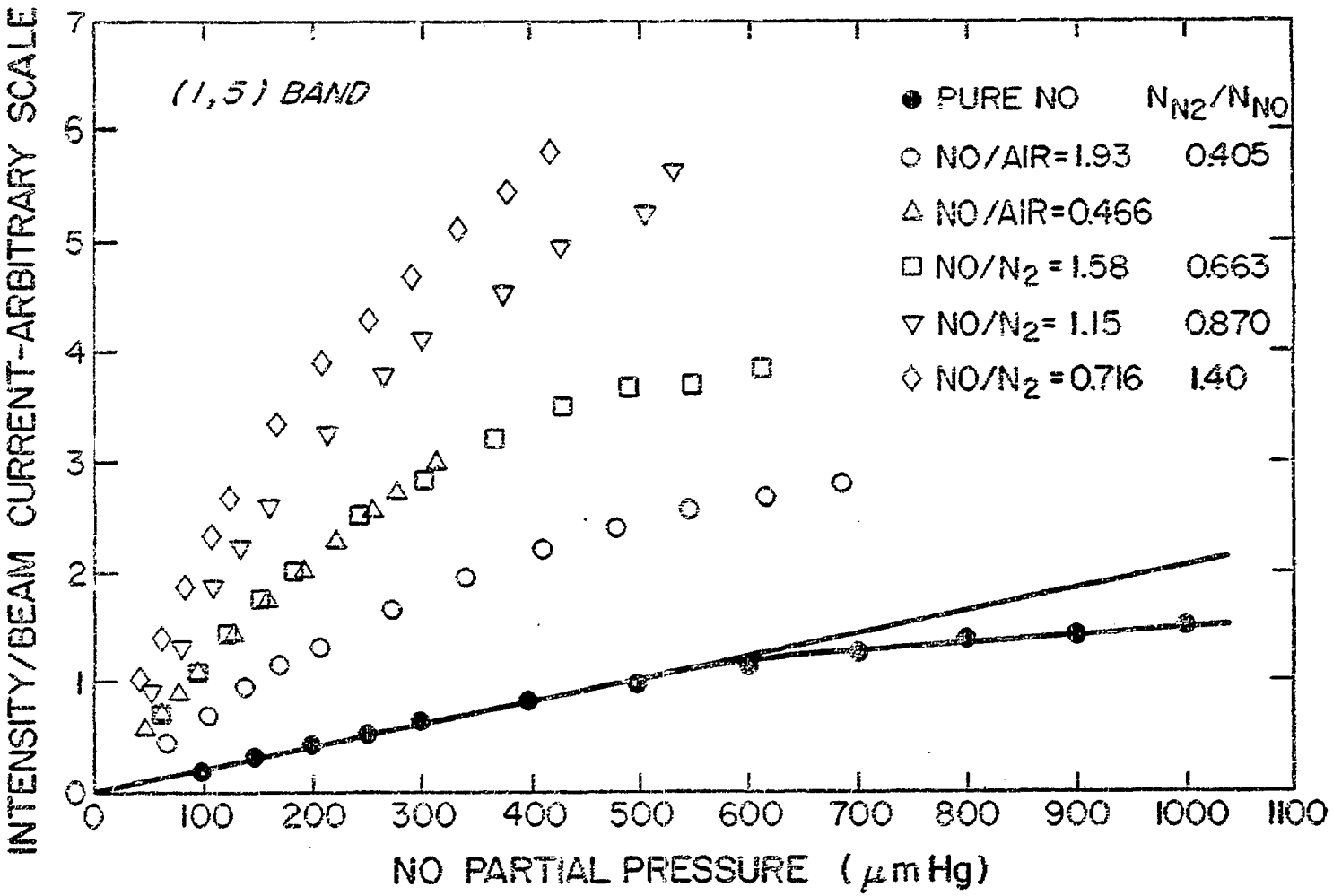

Figure 7. Intensity of NO γ (1,5) Band in Various Gas Mixtures

To determine if the variations of band intensities versus pressure in NO-air and NO-N_2 mixtures result from overlap of some other electronic transition, every known transition listed by Pearse and Gaydon[9] in N_2, N_2^+, O_2, and O_2^+ was investigated. The following bands of nitrogen could overlap the NO γ (0,2) band: the (14,25) band of the Lyman-Birge-Hopfield system, at 2481.7 Å, and the (0,[illegible]) band of the Herman-Kaplan system at 2471.4 Å. The NO γ (1,5) band may be overlapped by the (1,7) band of the nitrogen Fifth Positive system at 2681.2 Å, and the (0,4) band of Gaydon's T system at 2678.7 Å.

A spectral scan of the (0,2) band obtained with electron beam excitation of a gas mixture with an NO-air number density ratio of approximately 2 is shown in Figure 8. The band profile is the same as that observed in pure NO (Ref. 3).

No evidence of band overlap can be detected in any of the NO γ band profiles. In addition, the systems listed above have never been reported in excitation of N_2 by an electron beam. It is concluded that band overlap is not a likely cause for the observed intensities of the NO γ bands in NO-air and NO-N_2 mixtures.

It is particularly noteworthy that the intensity variations with pressure in NO-air and NO-N_2 mixtures are nearly identical when the data are examined at equal N_2 partial pressures. It is thus concluded that O_2 does not contribute significantly to the observed radiation intensities.

The intensity variations can be explained in terms of the excitation-emission analysis of Section II. The intensity divided by beam current for room-temperature mixtures is given by Eq (9), repeated below for convenience.

$$\frac{I}{J} = \frac{c_1}{1 - \frac{f_j A_{ji}}{A_{ji} + A} + \sum_k N_k/N_k'} \times \left\{ Q_o(v_e) N_j + \frac{Q_s(v_s) N_j \sum_k N_k Q_{kT}(v_e)}{\sum_k N_k Q_{ks}(v_s) + \lambda_s^2} + \sum_k \frac{Z'_{kj}}{J} N_j N_k^* \right\} \qquad (9)$$

As previously discussed, the influences of absorption can be neglected for the vibrational bands of interest here; hence, f_j is set equal to zero.

If collisions between ground state NO molecules and excited species contribute significantly to the observed radiation, then the intensities should very quadratically with the gas pressure, especially at low

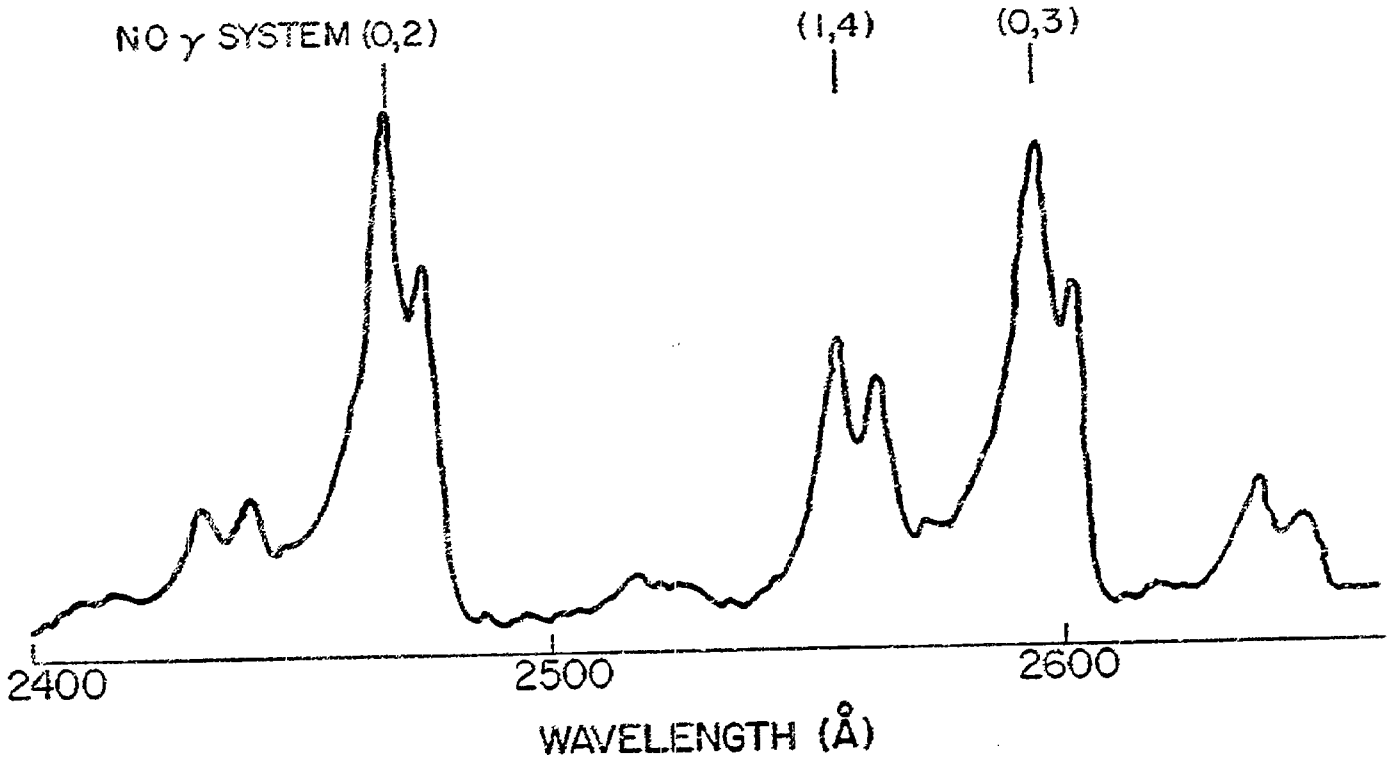

Figure 8. Spectral Scan of NO γ System in 67% NO, 33% Air

pressures where collision quenching can be ignored. Such a quadratic variation is not observed (Figures 6 and 7); hence, excitation by excited molecular and atomic species is ignored.

It is known that N_2 has a large total cross section for ionization[4] so that it can be assumed that N_2 dominates the production of secondary electrons. In addition, because of the low excitation energy of the $NO(A^2\Sigma)$ state, it is assumed that secondary electrons are lost primarily because of their collisions with ground state NO molecules. It is consistent with the latter assumption to assume that the range of secondary electrons is short in mixtures containing NO so that the secondary electron diffusion term in the denominator of the second term in Eq (9) can be neglected. Hence, Eq (9) becomes

$$\frac{I}{J} = \frac{c_1}{1 + \sum_k N_k/N'_k} \left\{ Q_O(v_e) N_{NO} + Q_{N_2,T}(v_e) N_{N_2} \right\} \tag{12}$$

or

$$\frac{I}{I'_O} = 1 + \frac{Q_{N_2,T}(v_e)}{Q_O(v_e)} \frac{N_{N_2}}{N_{NO}} \tag{13}$$

where I'_O is the intensity which would be observed if there were no contribution due to excitation by secondary electrons. Note that this analysis ignores all effects of collisions of particles with the container walls.

To test the validity of Eq (13), the data of Figures 6 and 7 are presented in Figure 9 as I/I'_O versus N_{N_2}/N_{NO} for several total pressures. Good agreement with Eq (13) is noted; the slope of the variation of I/I'_O yields a ratio of cross sections, $Q_{N_2,T}/Q_O$, of 3.28. The two data points obtained with air at a N_{N_2}/N_{NO} ratio of 1.67 do not correlate with the other data. This may be due to the presence of quenching mechanisms involving molecular oxygen which would not be present in a flowing system. For example, the reaction $NO + O \rightarrow NO_2 + h\nu$ may occur with sufficient frequency to reduce the number of NO molecules available for excitation by the primary electrons.

The calibration results are significant since they indicate that secondary electrons provide the predominant excitation of NO in mixtures containing N_2. This is not observed in pure NO because the yield of secondary electrons is much greater in collisions between beam electrons and N_2 molecules than it is in collisions between electrons and NO molecules. However, since the intensities of both the (0,2) and (1,5) bands vary in the same manner with N_{N_2}/N_{NO} (Figure 9), there is no noticeable influence of the secondary excitation on the band intensity ratio. Hence, valid vibrational temperature data should be obtained by reducing the band intensity data with Eq (1).

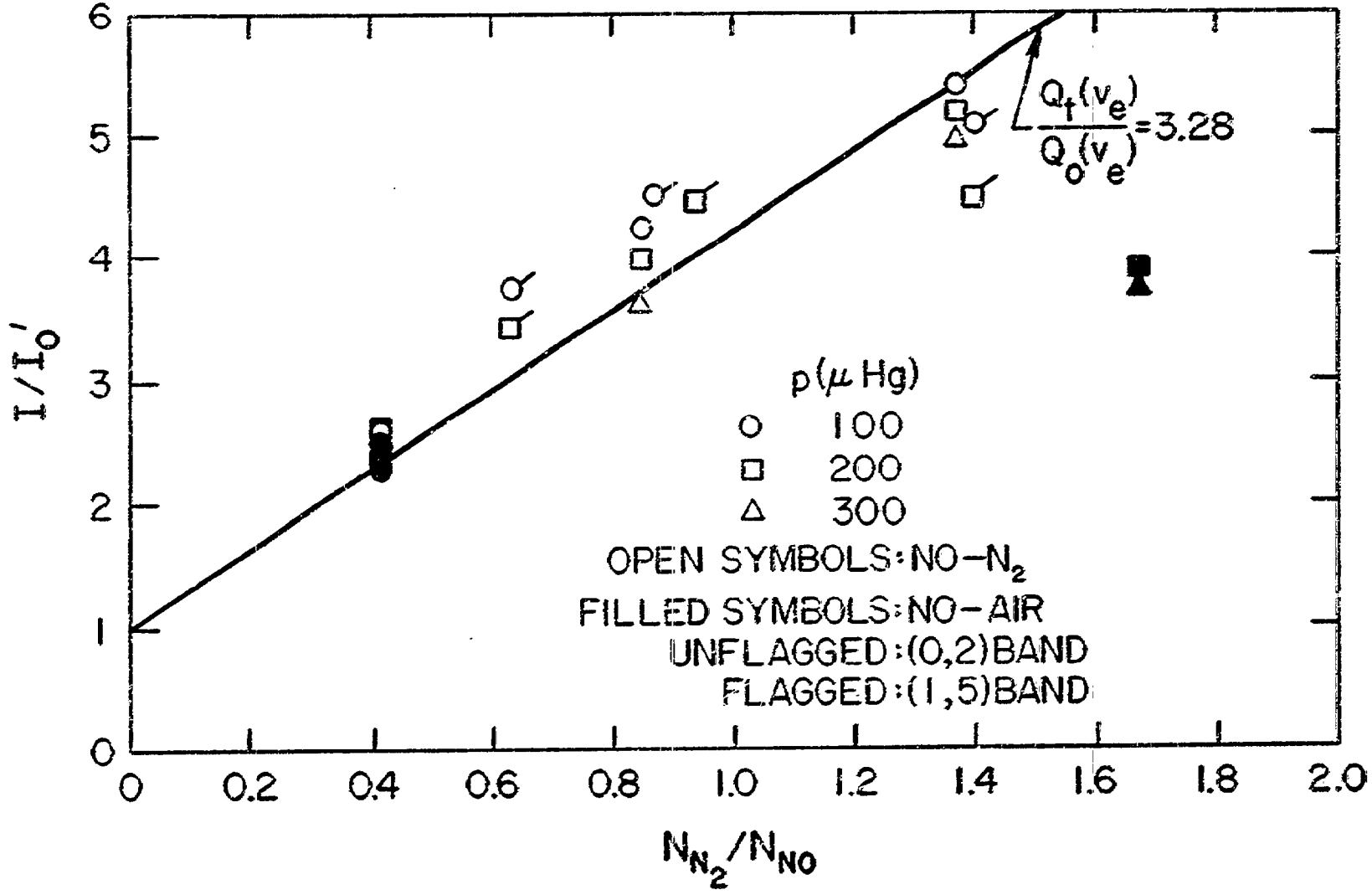

Figure 9. I/I_0' for NO γ (0,2) and (1,5) Bands

IV. APPARATUS AND PROCEDURES

A. WIND TUNNEL SYSTEM AND INSTRUMENTATION

The experimental studies were conducted in the 2-foot Electrogasdynamics Facility of the Air Force Flight Dynamics Laboratory. The facility consists of a direct current arc heater, a conical convergent-divergent nozzle exhausting to a free-jet cabin, and a pressure recovery system. For the experiments discussed here, nozzles with exit diameters of 7.0 and 19.4 inches were used. Further details of the facility may be found in Ref. 10. The typical tunnel run time in these studies was five minutes.

A pitot pressure-mass flow probe and a stagnation point calorimeter were employed in these tests. The pitot pressure-mass flow probe was mounted on a survey strut which allowed the probe to traverse the flow in a plane through the nozzle centerline. Pitot pressures were measured in 2-inch increments at three points below the centerline, on the centerline, and at four points above the centerline. Mass flow per unit area (ρu) was measured only on the centerline.

The stagnation point calorimeter was a water-cooled Gardon-type cylindrical probe with a hemispherical nose. Another Gardon-type calorimeter permanently installed on the tunnel centerline was used to obtain a continuous record of stagnation heating rate during the electron beam experiments.

The location of the various probes used with the 19-inch and 7-inch nozzles are summarized in Table I.

TABLE I. PROBE LOCATIONS IN INCHES DOWNSTREAM OF NOZZLE EXIT

Nozzle Dia. (in.)	Probe: Electron Beam	Pitot Pressure		$\dot{q}$
19	4.06	6.06	1.75	23.81
7	3.06	1.56	0.69	6.06

A portion of the tests included radial pitot pressure surveys at various axial stations in the 7-inch nozzle.

In addition to the flow field instrumentation, facility operating parameters were recorded during each run. These parameters included arc voltages, arc current, mass flow rate, water flow rates, and temperature rises.

The facility data were recorded through the on-line analog-digital data processor. Analog data signals from the tunnel instrumentation were entered through signal conditioning equipment, fed into the processor and computed, and the results stored in digital form on magnetic tape. Run identification and time reference data also were recorded with each data scan. At a specific test point, the data channels were recorded at a rate of 16 samples per second for a time interval of about 10 seconds. Immediately after the conclusion of a run, the individual scans for each data point were time averaged to give the final data at a test point.

B. ELECTRON BEAM SYSTEM

The electron beam system employed in the 2-foot EGF is identical to that described in Section II (Figure 3). The entire assembly is mounted inside the wind tunnel test cabin so that the electron beam was projected downward through the nozzle centerline at distances downstream of the nozzle exits as given in Table I. The electron beam power supplies and vacuum control console are located in a control panel adjacent to the tunnel. The beam generator is electrically isolated from the test cabin so that no special beam collecting device is required; that is, the tunnel test cabin serves as the beam receiver.

Electron beams with currents of approximately 20 mA at voltages near 40 kV were used for the tests. The beam currents were determined by measuring the voltage drop across a 570-Ω resistor in series with the beam current ammeter. The beam currents were monitored continuously during the wind tunnel run by displaying the voltage drop across the resistor on a X-Y plotter.

The optical system for collection of the vibrational temperature and number density data is shown schematically in Figure 10 and is described in detail in Ref. 2. Spectral resolution was accomplished with two 0.25-m Jarrell-Ash scanning spectrometers. The spectrometer gratings were ruled with 1180 lines/mm yielding a linear dispersion of 33 Å/mm and a maximum resolution near 1 Å.

The spectrometers and imaging optics were mounted on a traversing table which was attached to the tunnel test cabin. The table was moved in the vertical plane by a variable speed motor with a total traversing capability of 12 inches. A precision potentiometer was attached to the traversing table to provide an electrical signal proportional to the location of the field of view in the electron beam.

Both channel I and channel II intensities were measured with EMI 6256S photomultipliers. Various load resistors were employed in the anode circuitry of the photomultipliers and the resulting voltages were measured with PAR Model 124 lock-in amplifiers. The chopping frequency was 167 Hz. The signals from the lock-in amplifiers were displayed directly on two X-Y plotters.

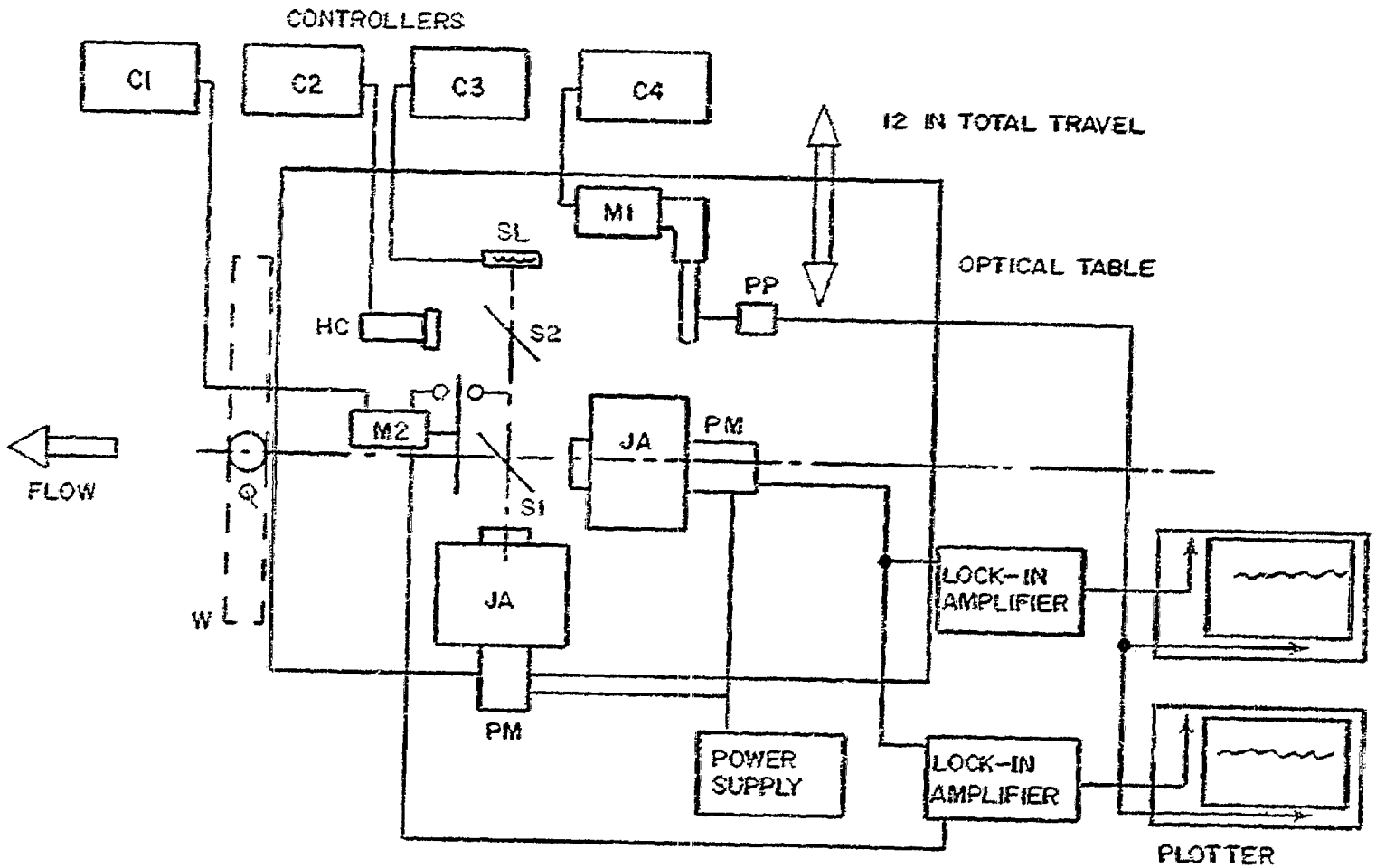

C1: CHOPPER CONTROL
C2: HOLLOW CATHODE CONTROL
C3: STANDARD LAMP CONTROL
C4: SCAN MOTOR CONTROL
HC: HOLLOW CATHODE LIGHT SOURCE

JA: 0.25 METER SPECTROMETER
M1: SCAN MOTOR
M2: CHOPPER MOTOR
PM: EMI 6256S PEOTOMULTIPLIER
PP: POSITION POTENTIOMETER

S1: SPLITTER
S2: SPLITTER
SL: STANDARD LAMP
W: WINDOW
Q: LENS

Figure 10. Instrumentation Schematic

C. TEST PROCEDURES

Prior to a wind tunnel test, the spectral locations of the spectrometers were set, a hollow-cathode discharge lamp which yields radiation in the NO γ bands was turned on, and the chopping wheel was started. The lock-in amplifiers were phase locked to the incoming signal and the light intensity was adjusted to provide photomultiplier outputs approximately equal to those expected during the run. The photomultipliers were allowed to fatigue under this condition for at least 30 minutes prior to the start of the wind tunnel run. This procedure was necessary to stabilize the gains of the photomultipliers and lock-in amplifiers, thus eliminating drifts in the relative sensitivities of the two channels during the course of the run.

Immediately before the start of a run, the tunnel vacuum system was started and a pressure of approximately 0.2 Torr was maintained in the test cabin region by leaking room air into the vacuum pumps. The electron beam was turned on and was scanned over the entire travel of the optical system. The signals from both channels were recorded on X-Y plotters to provide the calibration of the relative sensitivities of the two channels. During this scan, the test cabin pressure and electron beam current also were recorded. The beam was extinguished and the tunnel was started. The time lapse between the calibration exposure and the start of the run typically was less than one minute.

After the arc heater had achieved steady state conditions, a pitot pressure survey was taken and the centerline heat transfer rate was measured. At the conclusion of the probing, the electron beam was scanned in one direction. The spectrometers were then reset to measure the zero-reference signals and the beam was scanned in the opposite direction.

Run records typical of those obtained with the NO γ bands are shown in Figure 11.

D. DATA REDUCTION TECHNIQUES

To convert data such as that of Figure 11 to temperature and density, the sensitivities of both channels at each point along the beam must be obtained. Points at one inch intervals along the beam in the test flows were arbitrarily selected for data reduction.

To calibrate the sensitivities of the two data channels for nitric oxide measurements, a small test chamber was attached to the end of the drift tube of the electron beam generator. The chamber was evacuated with a mechanical vacuum pump and nitric oxide was continuously supplied to the chamber through a precision needle valve. The pressure in the chamber was measured with a variable reluctance pressure transducer. The electron beam was projected through the test chamber and captured in a water-cooled 90° elbow. The entire chamber was isolated

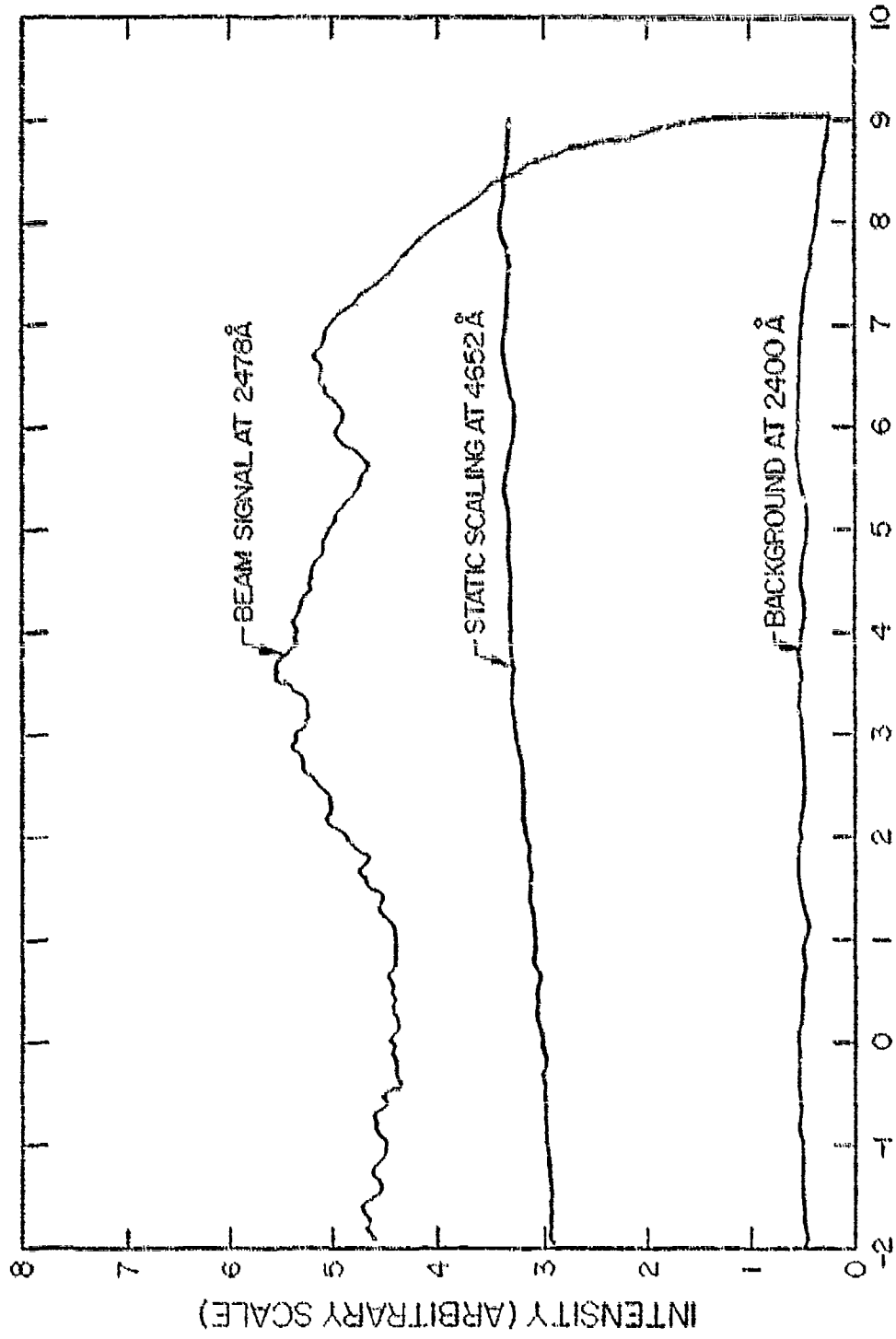

Figure 11. Typical Run Record

electrically from the drift tube so that it served as the beam current measuring device. The electro-optical system used for the calibration experiments duplicated that used in the wind tunnel runs. A photograph of the test chamber installation in the EGF is shown in Figure 12.

The intensities of the NO γ (0,2) and (1,5) bands at 2478 Å and 2680 Å were measured with channels I and II, respectively. The calibration constants, c_1, of Eq (12) were determined from the measured intensities, beam current, and pressure as

$$c_1 = \frac{(I/J)\left(1 + \sum_k N_k/N_k'\right)}{N_{NO}(1 + 3.28\ N_{N_2}/N_{NO})} \tag{14}$$

The ratio of nitrogen and nitric oxide number densities was determined by closing the valve which connected the vacuum pump to the test chamber and measuring the rate of increase of the chamber pressure both with NO flowing at the rate used during the calibrations and with no NO flow. The latter data were used to establish the rate of air leakage into the chamber.

To allow the calibration results to be properly applied to the wind tunnel experiments and to provide a continual check of the sensitivities of the two channels, the intensity of the (1,3) band of the N_2^+ first negative system at 4652 Å was measured with both channels during all pre-run and static test chamber calibrations. This band was chosen since its intensity under static conditions was nearly equal to those obtained from the (0,2) and (1,5) bands of nitric oxide.

The NO number densities were obtained from the intensities of the (0,2) and (1,5) bands with Eq (12) written in the following form:

$$N_{NO} = \frac{1 + \sum_k N_k/N_k'}{[S(T_v)/S(T_c)]c_1(1 + 3.28\ N_{N_2}/N_{NO})} \frac{(I/pJ)_{sc}^{N_2}}{(I/pJ)_c^{N_2}} \left(\frac{I}{J}\right) \tag{15}$$

where $(I/pJ)_{sc}^{N_2}$ and $(I/pJ)_c^{N_2}$ denote the intensities of the (1,3) band of the N_2^+ first negative system obtained during the static chamber and pre-run calibrations, respectively. The quenching density for NO, i.e. N_{NO}', was obtained from Ref. 11 and those for N_2 and O_2 were from Ref. 4. The quenching densities are summarized in Table II. The quenching factor was calculated employing species number densities resulting from the nonequilibrium calculations. Since the quenching factor was nearly unity for both the 19-inch and 7-inch nozzle tests, no iteration on the species concentrations was necessary. The vibrational temperature factor, $S(T_v)/S(T_c)$ was determined from the measured vibrational temperatures and Figure 2.

Figure 12. Test Chamber Installation in the 2-Foot EGF

TABLE II. QUENCHING CONSTANTS

Species	Quenching Species					
	NO		N_2		O_2	
	p'(Torr)	N'(cm^{-1})	p'(Torr)	N'(cm^{-1})	p'(torr)	N'(cm^{-1})
NO	2.35	7.56×10^{16}	1130*	3.64×10^{19}	0.85	2.73×10^{16}
N_2	-	-	1.90	6.11×10^{16}	1.77	5.70×10^{16}

*Average value for v' = 0 and v' = 1 levels of $NO(A^2\Sigma)$

The nitric oxide vibrational temperatures were determined from the ratio of measured (1,3) and (0,2) band intensities. To account for the relative sensitivities of the two channels, the measured ratios were scaled according to the ratio measured in the static test chamber. Hence, the intensity ratio was determined as

$$\frac{I_{1,3}}{I_{0,2}} = \frac{(I/J)_{II}}{(I/J)_{I}} \frac{0.765}{\left[I_{1,3}/I_{0,2}\right]_{sc}} \tag{16}$$

where the subscripts I and II denote the intensities of channels I and II, respectively, and 0.765 is the room-temperature vibrational band intensity ratio for channels with equal sensitivities (Figure 1).

The number densities of molecular nitrogen were determined from the measured intensities of the (0,1) and (1,2) bands of the N_2^+ first negative system at 4278 Å and 4236 Å, respectively. The (0,1) band intensity was measured with channel I, while that for the (1,2) band was measured with channel II. Since a pre-run calibration for each channel was easily possible by passing the electron beam through the tunnel test cabin under static pump-down conditions, the data reduction procedures for the N_2 measurements were simpler than those for the NO measurements.

The N_2 number densities were obtained from the measured band intensities with the procedure described in Ref. 1; that is,

$$N_{N_2} = \frac{1 + \sum_k N_k/N_k'}{\left[S(T_V)/S(T_C)\right]} \left(N_{N_2}\right)_C \frac{I/J}{(I/J)_C} \tag{17}$$

where $\left(N_{N_2}\right)_C$ is the N_2 number density of the pre-run calibrations. The quenching factor was determined from the species concentrations obtained from the nonequilibrium calculation with no iteration on the individual species concentrations. The quenching densities, N_k', for N_2 were obtained from Ref. 4 and are summarized in Table XI.

The N_2 vibrational temperatures were determined from the measured band intensities with the formula

$$\frac{I_{0,1}}{I_{1,2}} = \frac{(I/J)_{I}}{(I/J)_{II}} \frac{7.85}{\left[I_{0,1}/I_{1,2}\right]_C} \tag{18}$$

where 7.85 is the band intensity ratio for channels having equal sensitivities (Figure 1).

To minimize the influences of run-to-run variations in the data correlations, the measured number densities were nondimensionalized by the corresponding reservoir number densities. The reservoir values $[NO]_o$ and $[N_2]_o$ were determined from the reservoir composition obtained from the average reservoir enthalpy during the scan of the electron beam.

V. RESULTS AND DISCUSSIONS

A. THEORETICAL ANALYSES

For comparison with the experimental results, the inviscid flow properties at various stations in the EGF nozzles were obtained with a nozzle-flow computer program which is described in Ref. 2. The program computes the numerical expansion of a reacting gas mixture starting from an equilibrium reservoir through a streamtube of arbitrary geometry. The rotational and translational degrees of freedom are assumed to be equilibrated throughout the expansion. The vibrational energy mode can be assumed to be either in equilibrium with the translational energy mode or frozen at the reservoir condition. The electronic energy mode is assumed to be equilibrated with the vibrational energy mode. The chemistry may be assumed to be frozen at the reservoir state, remain in equilibrium, or to proceed in a nonequilibrium fashion through the expansion. Corrections for the growth of the nozzle boundary layer are included in the analysis.

B. NOMINAL RUN CONDITIONS

Wind tunnel data were obtained at three nominal run conditions. The nozzle throat diameter was 0.4375 inch. For conditions 2 and 3, the heater was operated at reservoir pressures of 350 and 500 psia and nominal enthalpies of 3500 and 2500 Btu/lb, respectively. For condition 1, another arc heater was employed which supplied a nominal enthalpy of 6000 Btu/lb with a reservoir pressure of 250 psia.

The nominal reservoir conditions are summarized in Table III. The range of enthalpies (in Btu/lb) employed were 5599 to 5931 for condition 1, 2885 to 3480 for condition 2, and two enthalpy ranges for condition 3, 2127-2301 and 3694-3936.

C. PROBE DATA

The pitot pressure data are summarized in Figures 13-17. It should be noted that little run-to-run variation in the pitot pressure was obtained.

TABLE III. NOMINAL RESERVOIR CONDITION SUMMARY

Run Condition	p_o (psia)	H_o (Btu/lb)	T_o (K)
1	250	6000	6564
2	350	3500	4714
3	500	2500	3973

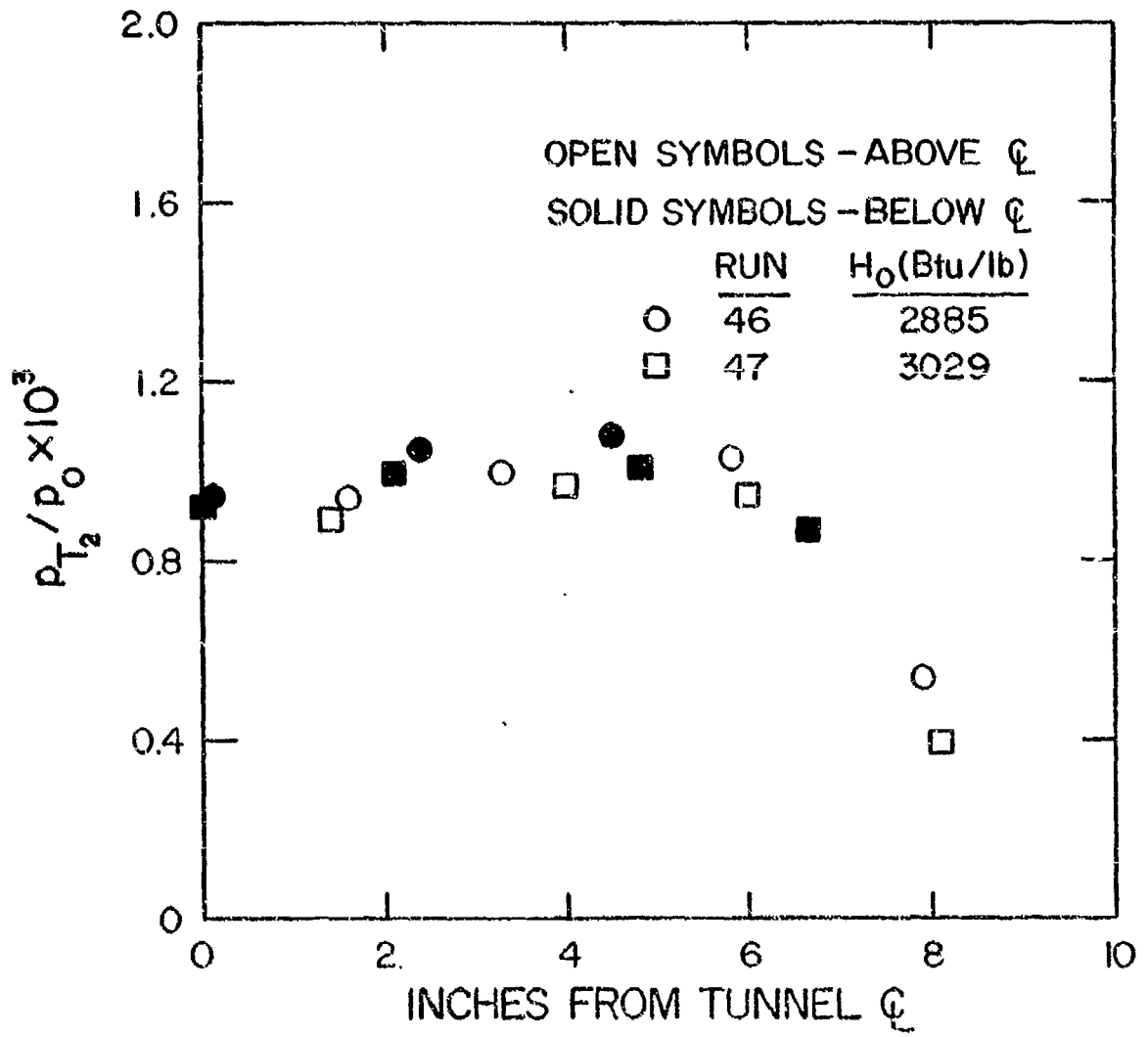

Figure 13. Pitot Pressure Surveys at Run Condition 2; 19-Inch Nozzle; p_o = 350 psia

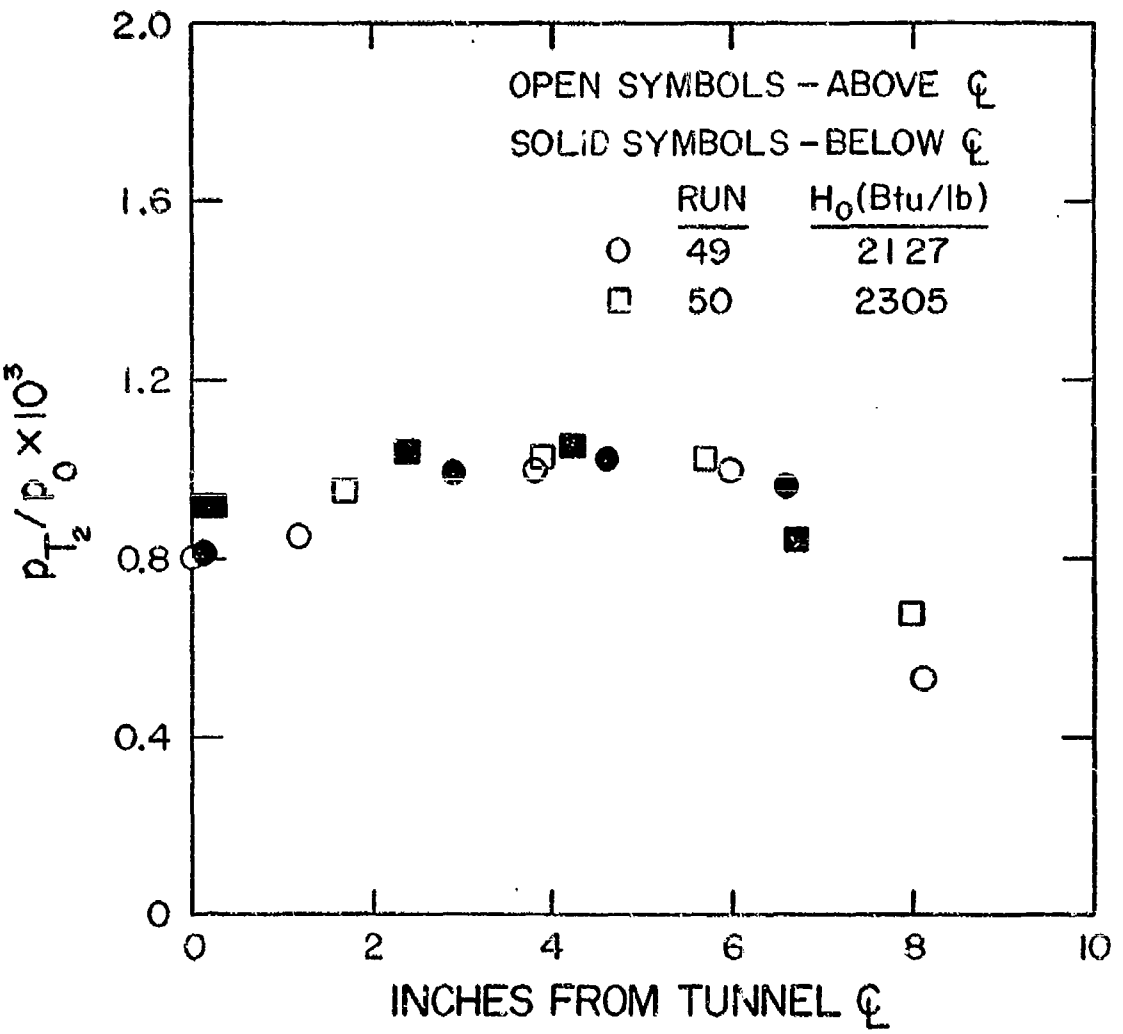

Figure 14. Pitot Pressure Surveys at Run Condition 3; 19-Inch Nozzle; p_o = 500 psia

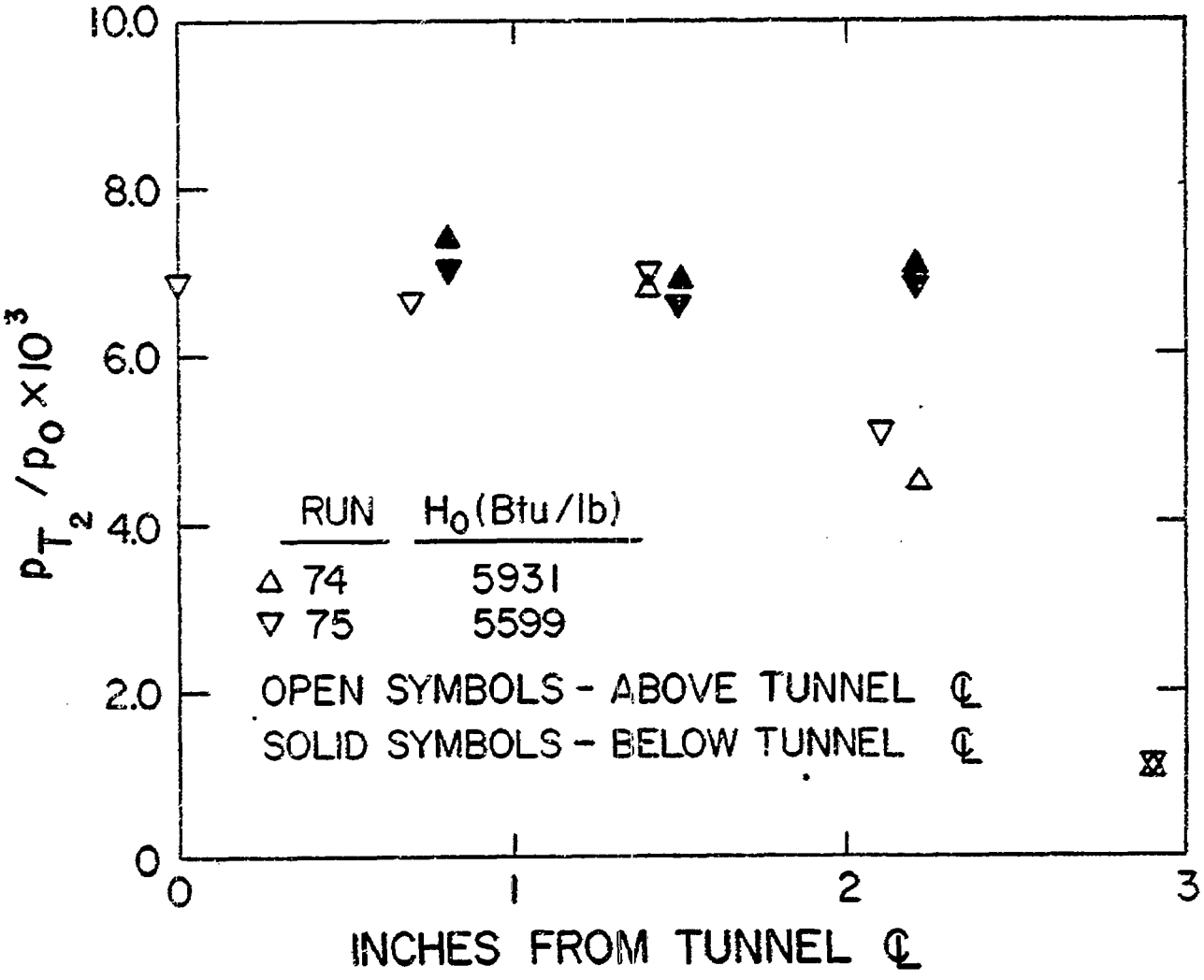

Figure 15. Pitot Pressure Surveys at Run Condition 1; 7-Inch Nozzle; p_0 = 250 psia

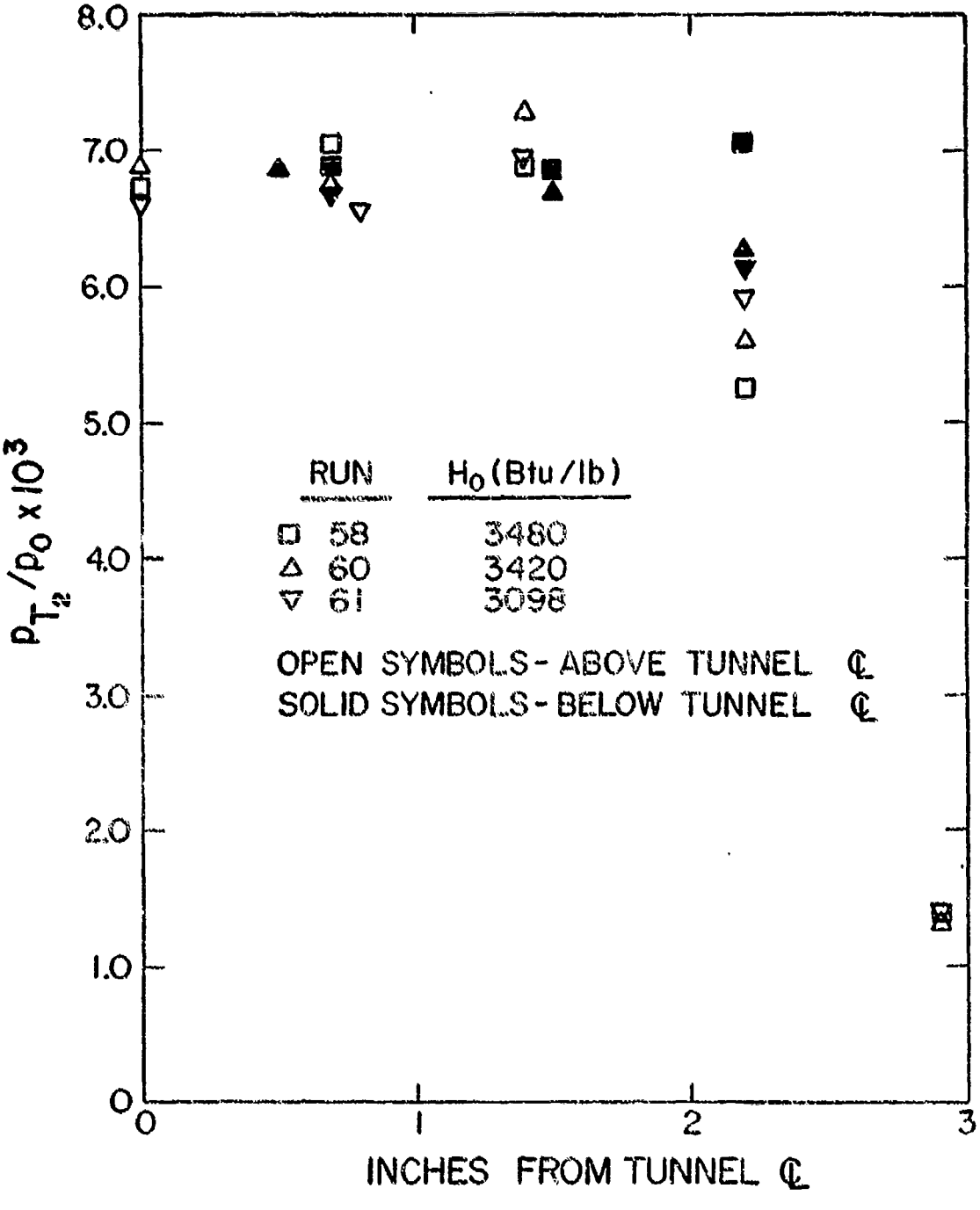

Figure 16. Pitot Pressure Surveys at Run Condition 2; 7-Inch Nozzle; p_o = 350 psia

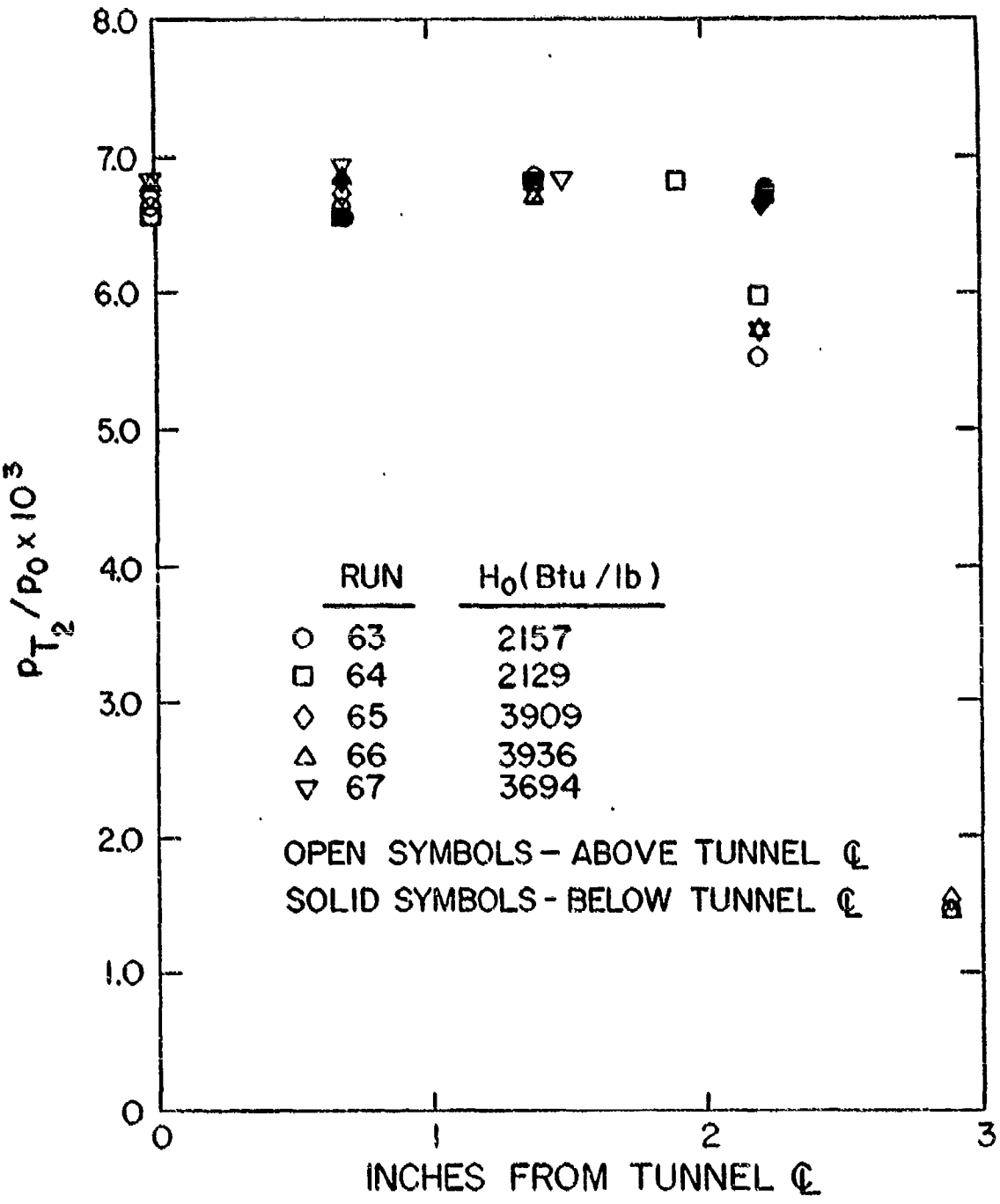

Figure 17. Pitot Pressure Surveys at Run Condition 3; 7-Inch Nozzle; p_0 = 500 psia

Axial surveys of the pitot pressures were taken to determine the pitot pressure gradients throughout the region of measurement in the 7-inch nozzle. The data are summarized in Figures 18-21. The axial variations of pitot pressure shown in Figure 21 were used to determine the pitot pressures at the electron beam location to allow accurate comparisons of the experimental data with the results of the theoretical predictions.

Similar axial surveys of pitot pressure in the 19-inch nozzle are reported in Ref. 1, where it is shown that the axial variations are negligible for all run conditions in the 19-inch nozzle.

D. VIBRATIONAL TEMPERATURES

The measured vibrational temperatures of molecular nitrogen nondimensionalized by the reservoir temperature are summarized for the 7-inch nozzle in Figure 22. Excellent run-to-run repeatability was obtained and little data scatter was observed.

The vibrational temperature ratio of approximately 0.4 obtained at run conditions 1 and 3 is in agreement with vibrational temperature data obtained in the 19-inch nozzle as reported in Ref. 1.

The behavior of the nitrogen vibrational temperature distribution near the boundary layer edge is expected and indicates the tendency for a greater degree of vibrational relaxation to occur in the low-speed portions of the flow field. Similar effects were observed in the 19-inch nozzle.[1] Note, however, at all run conditions there is a sizable degree of vibrational nonequilibrium.

The measured vibrational temperatures of nitric oxide nondimensionalized by the reservoir temperatures are summarized for the 7-inch and 19-inch nozzles in Figures 23 and 24.

Vibrational temperature data could not be obtained for nitric oxide at run condition 1, for either nozzle, because of the combination of an extremely low nitric oxide concentration and a sizable background signal. This result is expected, however, since estimates of the nitric oxide concentrations at these run conditions show that the nitric oxide partial pressure is less than 0.0001 Torr. Since the low density limit for the measurement technique is near 0.001 Torr, the nitric oxide concentrations at these run conditions are more than an order of magnitude below the detectable limit. The measurement problem at run condition 1 is compounded by the background radiation which is approximately twice as intense as those at run conditions 2 and 3.

The sensitivities of the ratios of band intensities in the NO γ system place extreme requirements on the accuracy of the intensity measurement system (Figure 1). For example, for the (1,5)/(0,2) band combination, an error in the measured ratio of ±10% will yield an error

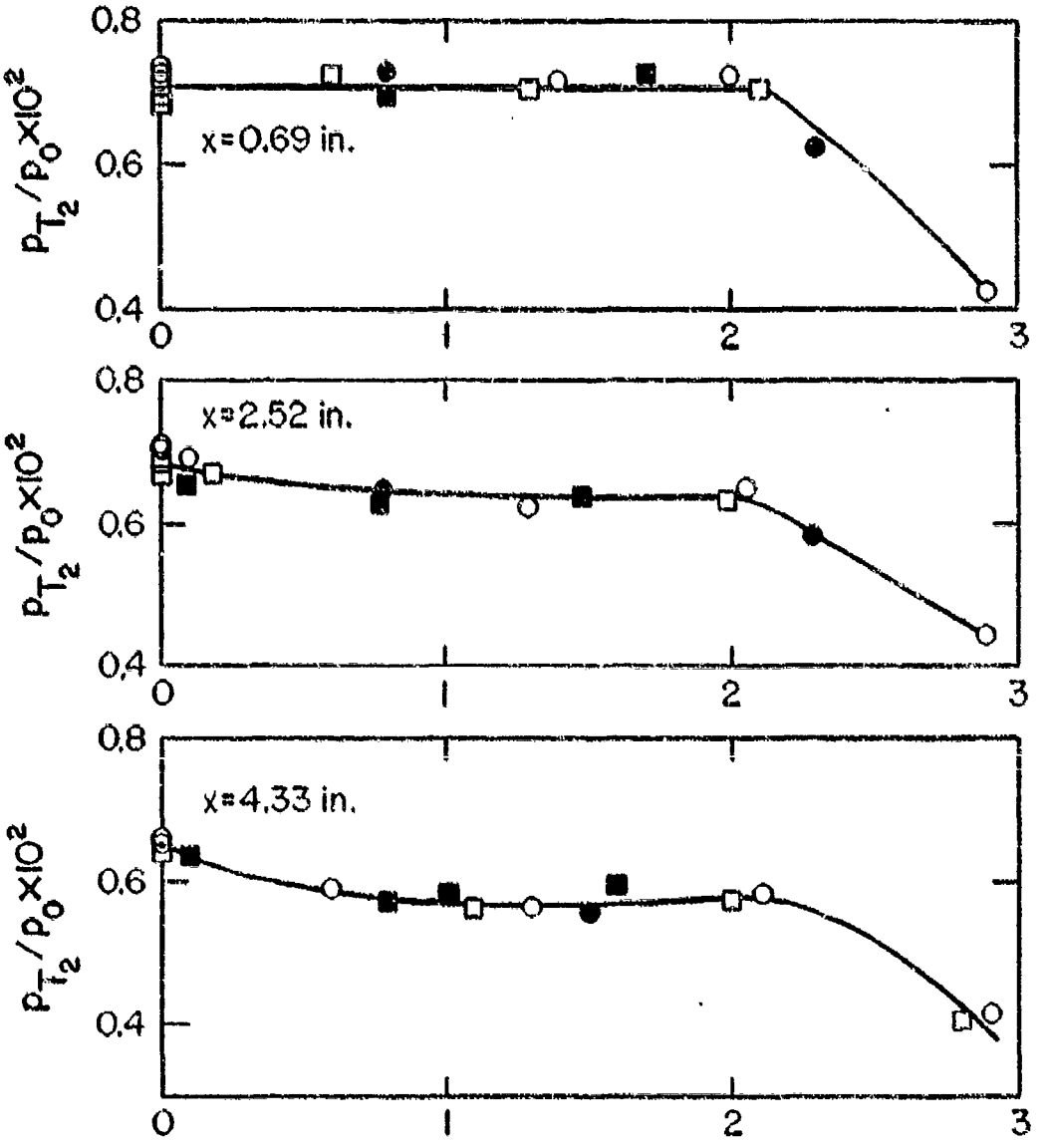

	RUN	H_0(Btu/lb)	P_0(psia)
o	76	6055	251
□	77	5416	252

OPEN SYMBOLS – ABOVE TUNNEL ℄
SOLID SYMBOLS – BELOW TUNNEL ℄

Figure 18. Pitot Pressure Surveys at Various Axial Stations - Run Condition 1, 7-Inch Nozzle

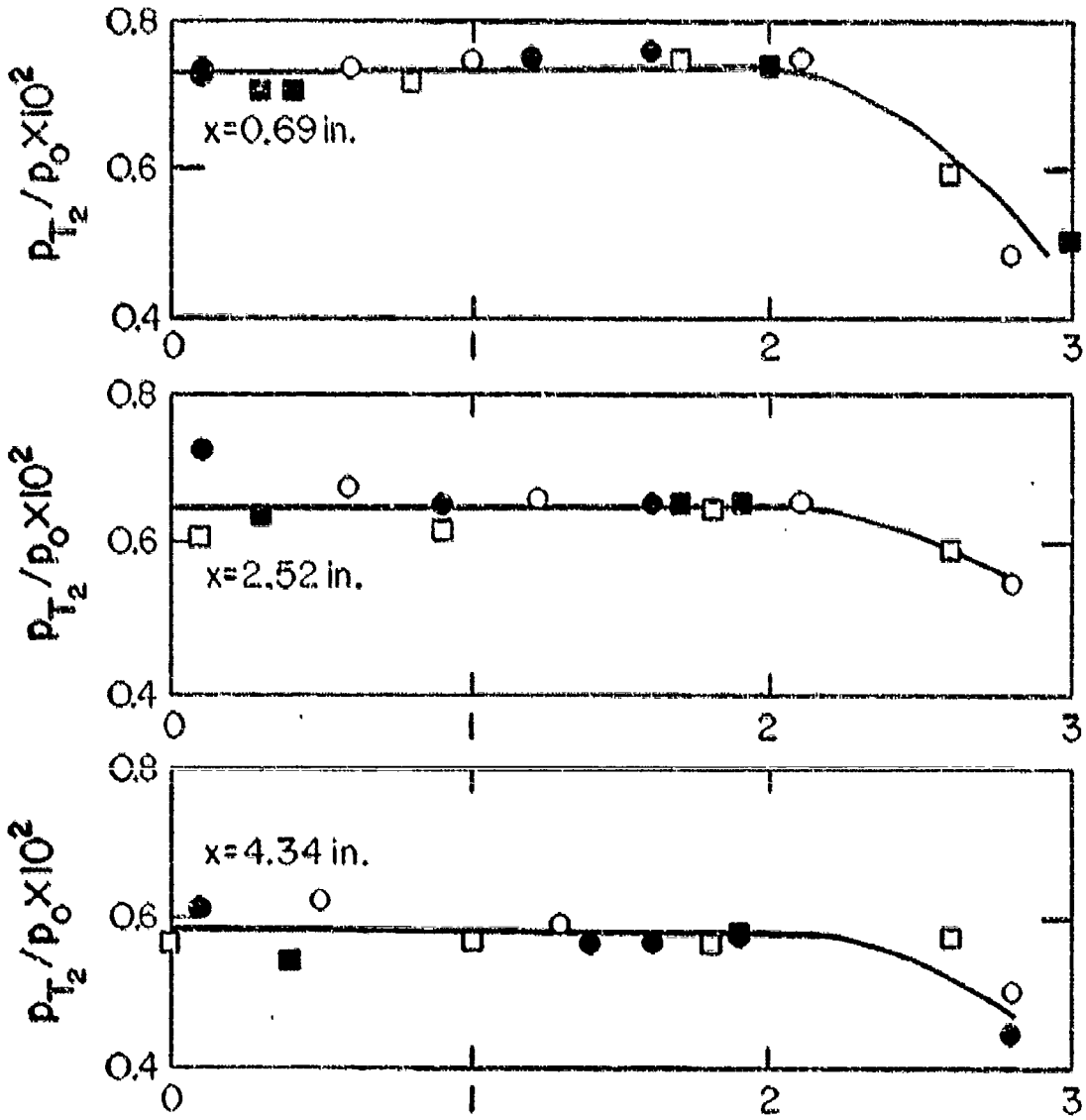

	RUN	H_0(Btu/lb)	P_0(psia)
○	78	3078	351
□	79	3755	354

OPEN SYMBOLS – ABOVE TUNNEL ℄
SOLID SYMBOLS – BELOW TUNNEL ℄

Figure 19. Pitot Pressure Surveys at Various Axial Stations - Run Condition 2, 7-Inch Nozzle

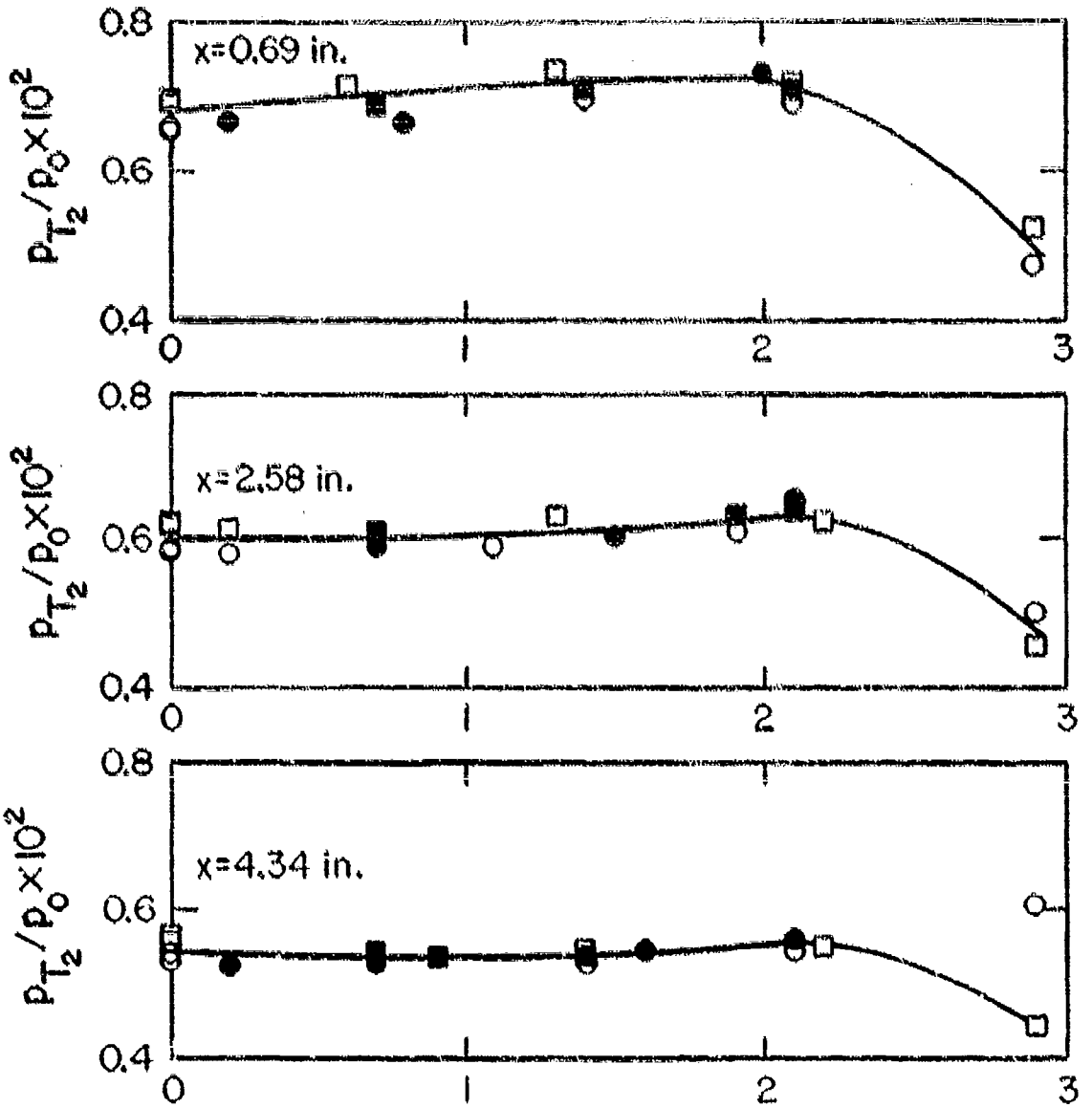

	RUN	H_o(Btu/lb)	P_o(psia)
○	80	2769	502
□	81	3566	503

OPEN SYMBOLS - ABOVE TUNNEL ℄

SOLID SYMBOLS - BELOW TUNNEL ℄

Figure 20. Pitot Pressure Surveys at Various Axial Stations - Run Condition 3, 7-Inch Nozzle

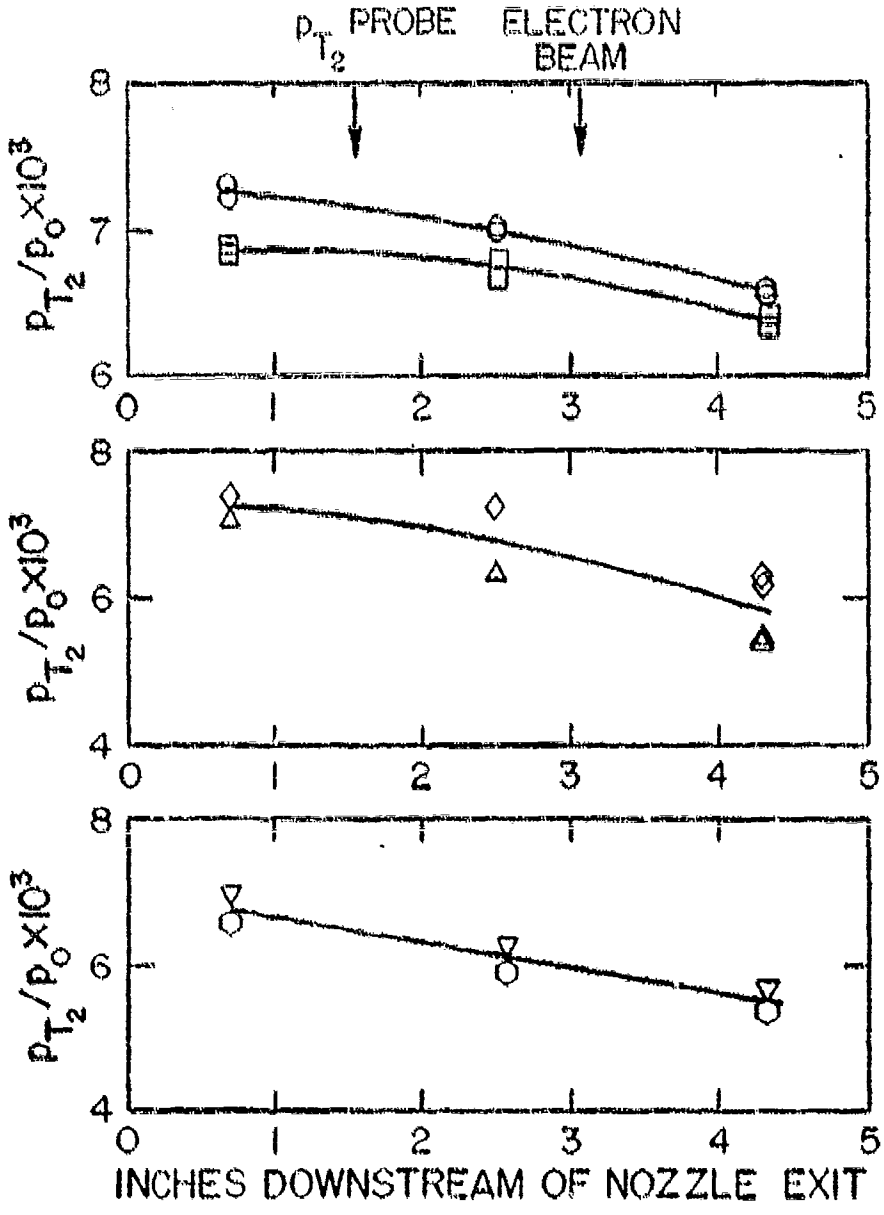

	RUN	H_0(Btu/lb)	P_0(psia)
○	76	6055	251
□	77	5416	252
◇	78	3078	351
△	79	3755	354
⬡	80	2769	502
▽	81	3566	503

Figure 21. Axial Centerline Pitot Pressures; 7-Inch Nozzle

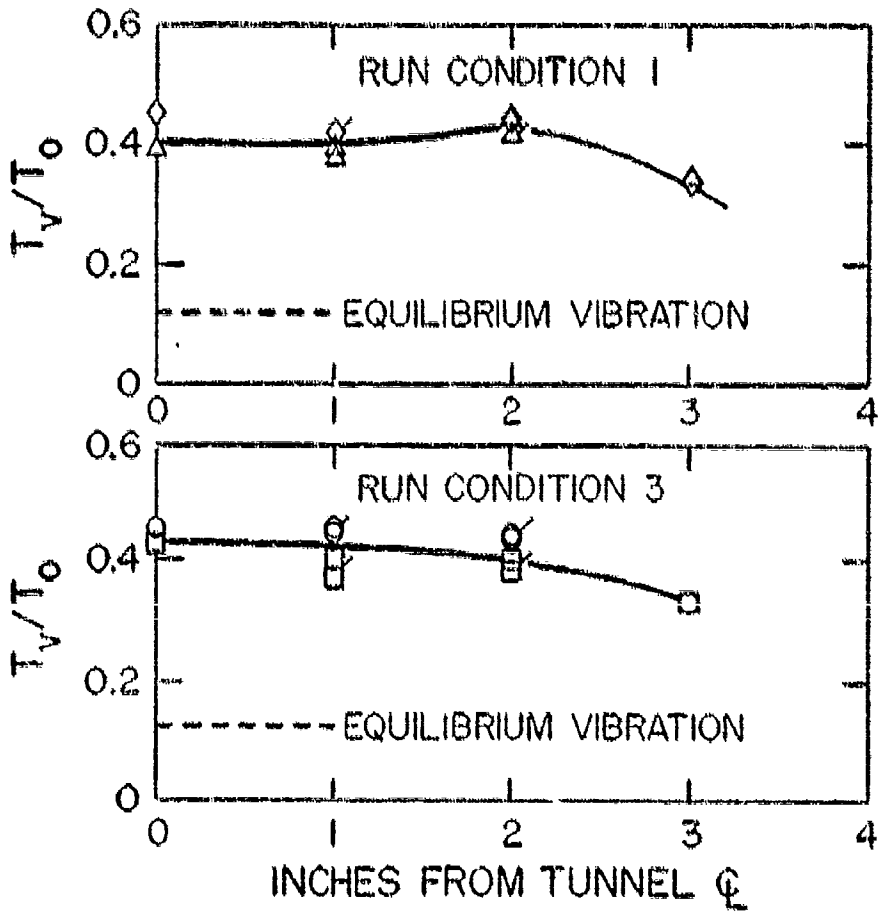

	RUN COND	RUN	H_o (Btu/lb)	T_o (°K)
△	1	74	5931	6529
◇	1	75	5599	6346
○	3	64	2129	3672
□	3	65	3909	5131

FLAGGED SYMBOLS - BELOW ℄
UNFLAGGED SYMBOLS - ABOVE ℄

Figure 22. N_2 Vibrational Temperatures; 7-Inch Nozzle

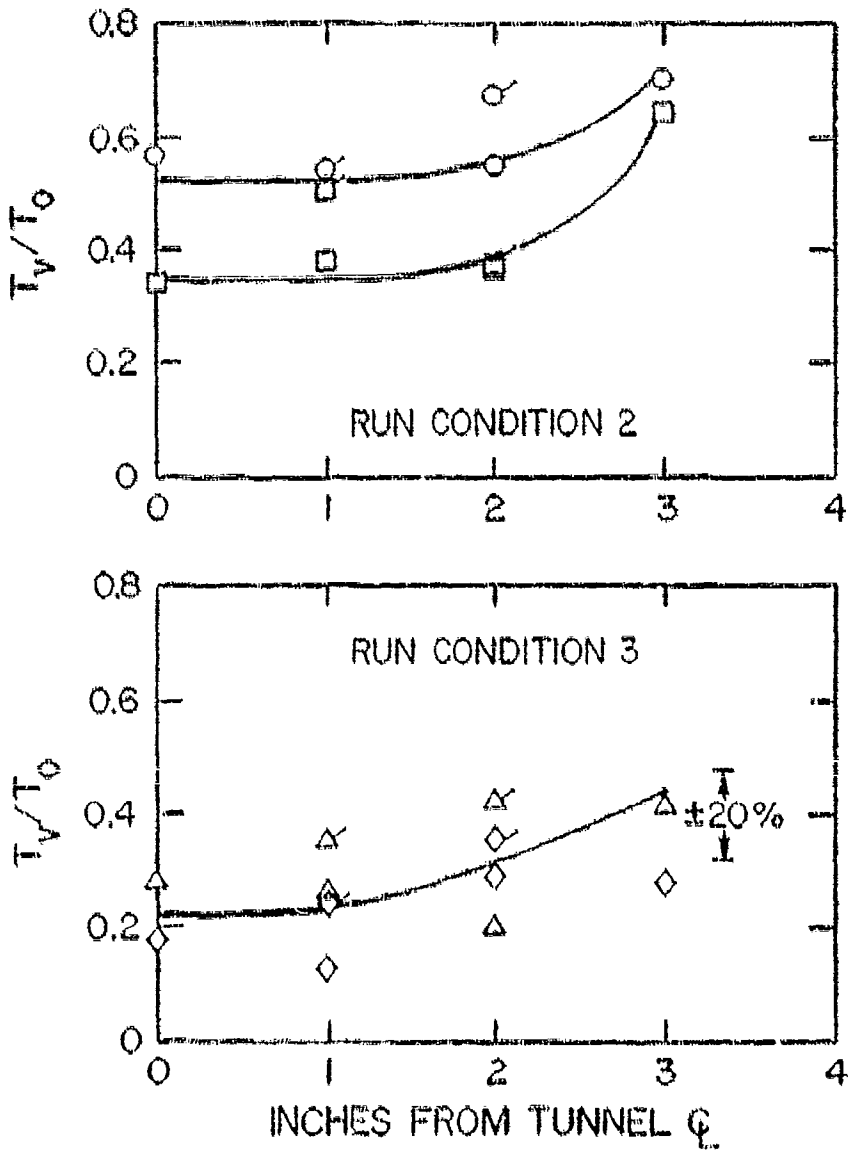

	RUN COND	RUN	H_o (Btu/lb)	T_o (°K)
○	2	60	3420	4651
□	2	62	3043	4360
◇	3	66	3936	5155
△	3	67	3694	4944

FLAGGED SYMBOLS – BELOW ℄
UNFLAGGED SYMBOLS – ABOVE ℄

Figure 23. NO Vibrational Temperatures; 7-Inch Nozzle

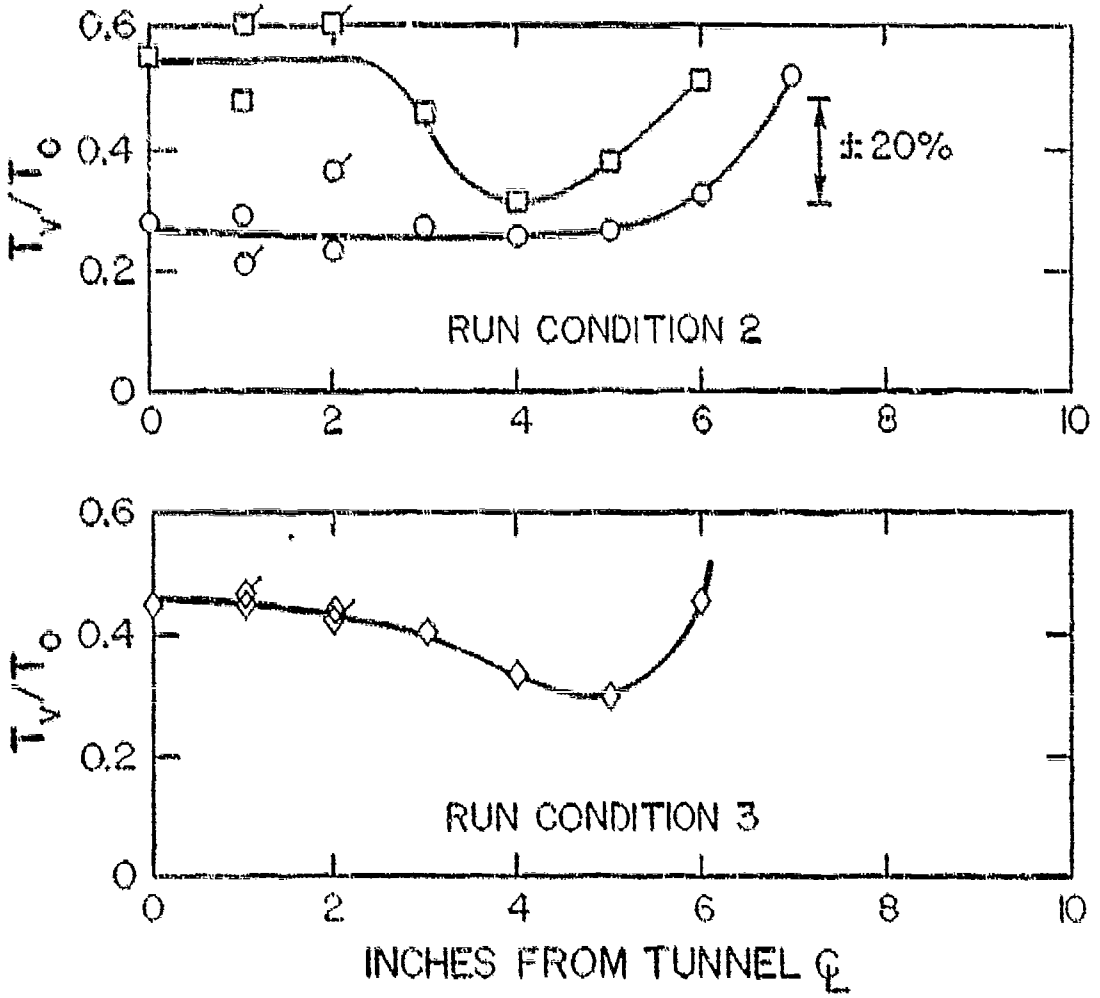

	RUN COND	RUN	H_o (Btu/lb)	T_o (°K)
○	2	46	2885	4235
□	2	47	3029	4346
◇	3	49	2127	3625

FLAGGED SYMBOLS - BELOW ℄
UNFLAGGED SYMBOLS - ABOVE ℄

Figure 24. NO Vibrational Temperatures; 19-Inch Nozzle

in vibrational temperature of ±25%. Hence, the accuracy of the NO vibrational temperatures is estimated to be ±20%.

The scatter in the data of Figures 23 and 24 is generally within the ±20% accuracy expected for these measurements. The averages of the nitric oxide vibrational temperatures fall into two general categories: a vibrational temperature ratio near 0.4, and a ratio near 0.25. A close coupling between the vibrational energy modes of the various species is expected due to the extremely rapid vibration-vibration energy exchanges which occur. However, an interesting trend in the higher vibrational temperature data obtained in the 19-inch nozzle is evident in Figure 24. These higher temperature data show a definite tendency for the vibrational temperatures to decrease near the edge of the boundary layer. These variations may be related to the mechanisms which lead to chemiluminescence caused by the reaction $NO + O \rightarrow NO_2 + h\nu$. Relatively strong radiation due to chemiluminescence has been observed at various run conditions,[12] and it is likely that the associated chemical reaction will perturb the nitric oxide vibrational population distribution.

The behavior of the nitric oxide vibrational temperature near the boundary layer edge is in agreement with that obtained for the molecular oxygen vibrational temperature variations.[2] However, the changes in both the molecular oxygen and nitric oxide vibrational temperatures near the boundary layer edge are opposite to those changes obtained for the N_2 vibrational temperature. It is expected that a greater degree of vibrational relaxation will occur within the lower-speed portions of the boundary layer. Although the amount of relaxation in the boundary layer is small, decreases in the vibrational temperatures are expected rather than increases noted in Figures 23 and 24. As discussed in Ref. 2, these vibrational temperature variations might result from a coupling between the vibrational relaxation and the fast nitric oxide shuffle reactions.

E. NUMBER DENSITIES

The measured molecular nitrogen concentration profiles for the 7-inch nozzle are given in Figures 25 and 26. The theoretically predicted concentrations are also included.

The run-to-run repeatability and scatter within a given run are within the ±10% accuracy expected for these measurements.

The nitrogen number density data obtained at run condition 1 with the 7-inch nozzle are in good agreement with the results of the theoretical predictions.

The nitrogen number density data obtained at run condition 3 is in poor agreement with the results of the theoretical predictions. It should be noted that there is little scatter in the run-to-run variations

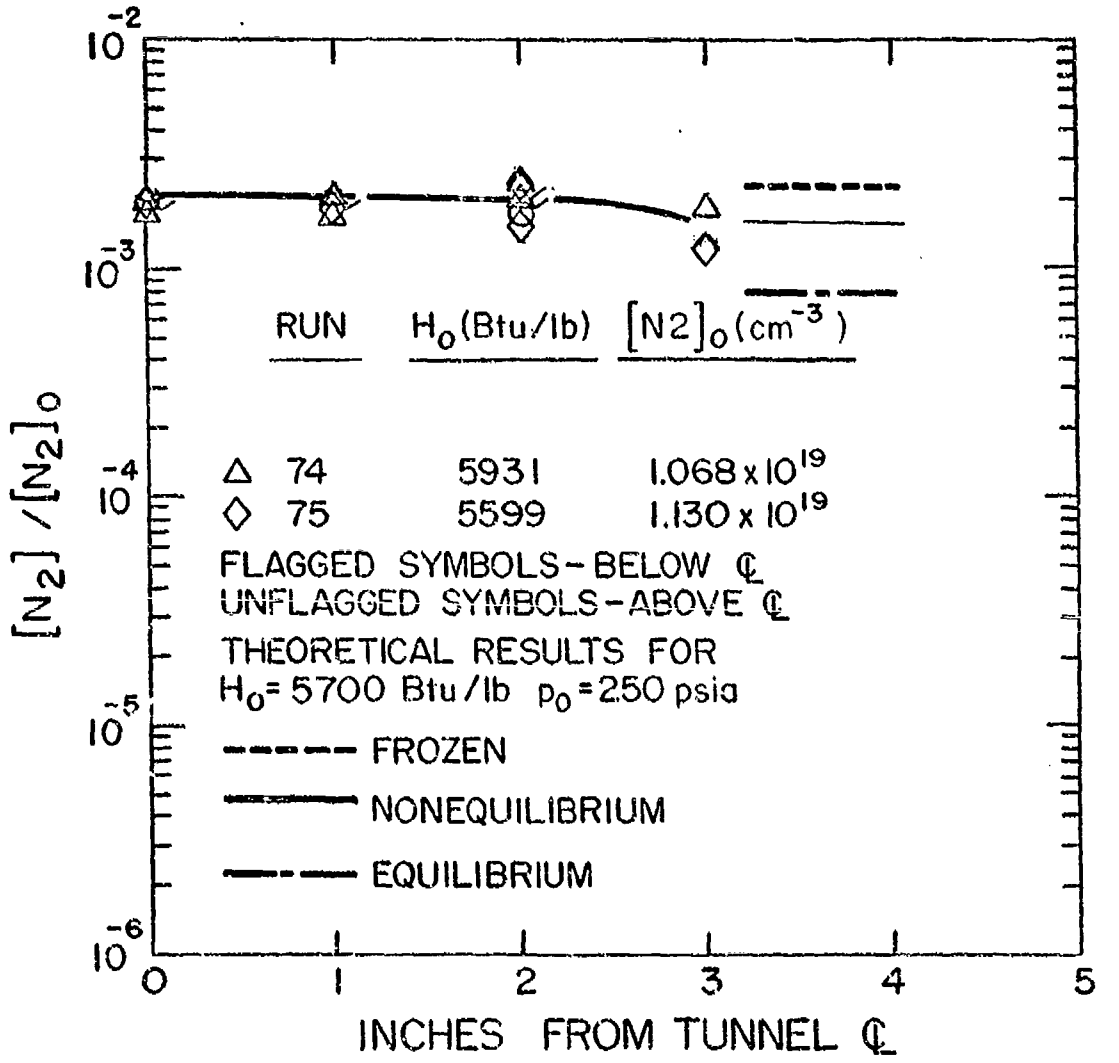

Figure 25. N_2 Number Densities at Run Condition 1; 7-Inch Nozzle

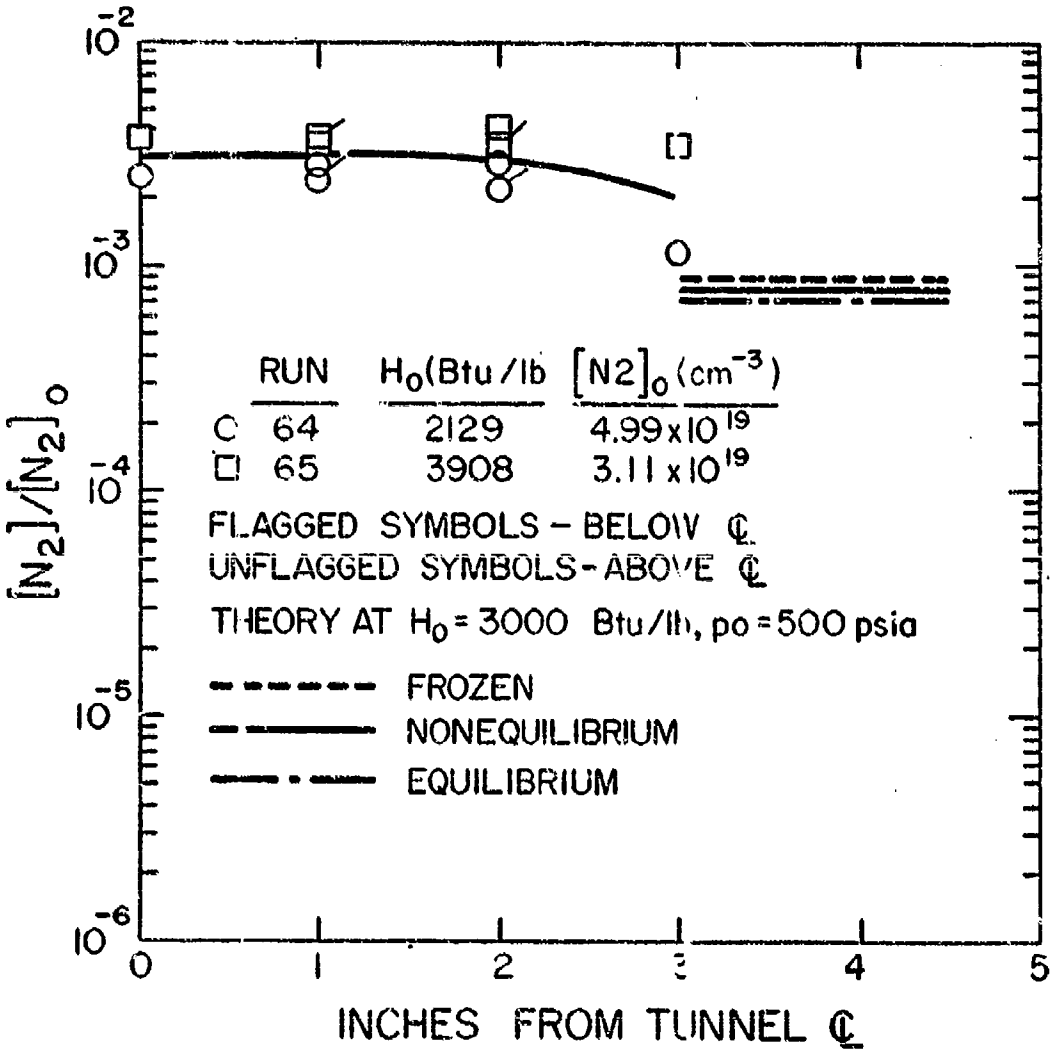

Figure 26. N_2 Number Densities at Run Condition 3; 7-Inch Nozzle

and that the differences between the theoretical and experimental results are well outside the ±10% error band expected for the data.

The experimental techniques give redundancy in the number density measurements. The number densities can be obtained either from the intensities of the (0,1) or the (1,2) vibrational bands. The number densities obtained from these two bands are coupled only through the density correction factor, $S(T_v)$, which must be obtained from the vibrational temperature measurement. As seen in Figure 2, this coupling is relatively weak. In all cases, the nitrogen number densities obtained from the two vibrational bands agreed with an error less than ±2%. Hence, it is concluded that the differences between the theoretical and experimental predictions of the nitrogen number densities are not a result of systematic errors in the measurement of the nitrogen concentration.

Many factors enter into the comparisons of the theoretical and experimental results. The data are nondimensionalized by the reservoir nitrogen number densities, which are determined from thermochemical calculations assuming complete equilibrium in the reservoir. In addition, the theoretical predictions are based on the centerline pitot pressure values, while both axial and radial pitot pressure variations exist. The differences between the theoretical and experimental nitrogen number densities may result from cumulative errors in these factors. Note that there is little variation in the predicted nitrogen number densities due to changes in the assumed chemical model, since molecular nitrogen behaves almost as an inert chemical species in the temperature range of these tests.

The measured nitric oxide species concentrations are compared with the results of the theoretical predictions in Figures 27-30. Except for the data obtained with the 19-inch nozzle at run condition 3 (Figure 30), the measured number densities are consistently below the predicted values, indicating a greater degree of chemical recombination than predicted by theory. Nitric oxide concentrations resulting from assuming chemically frozen and chemical nonequilibrium only are included in Figures 27-30. The theoretical results assuming chemical equilibrium in the nozzle expansion give nitric oxide concentrations less than 2×10^{-5} vol %.

Generally, good run-to-run repeatability and little data scatter within a given run were experienced with the nitric oxide number density measurements. The number densities shown in Figures 27-30 are those obtained from the intensity of the NO γ (0,2) band. The number densities obtained from the NO γ (1,5) band generally agreed with those from the (0,2) band to within 8%.

The factors which affect the comparisons of the theoretical and experimental nitrogen densities also influence the comparisons for the nitric oxide number densities. However, the consistency of the differences between the measured and predicted nitric oxide concentrations

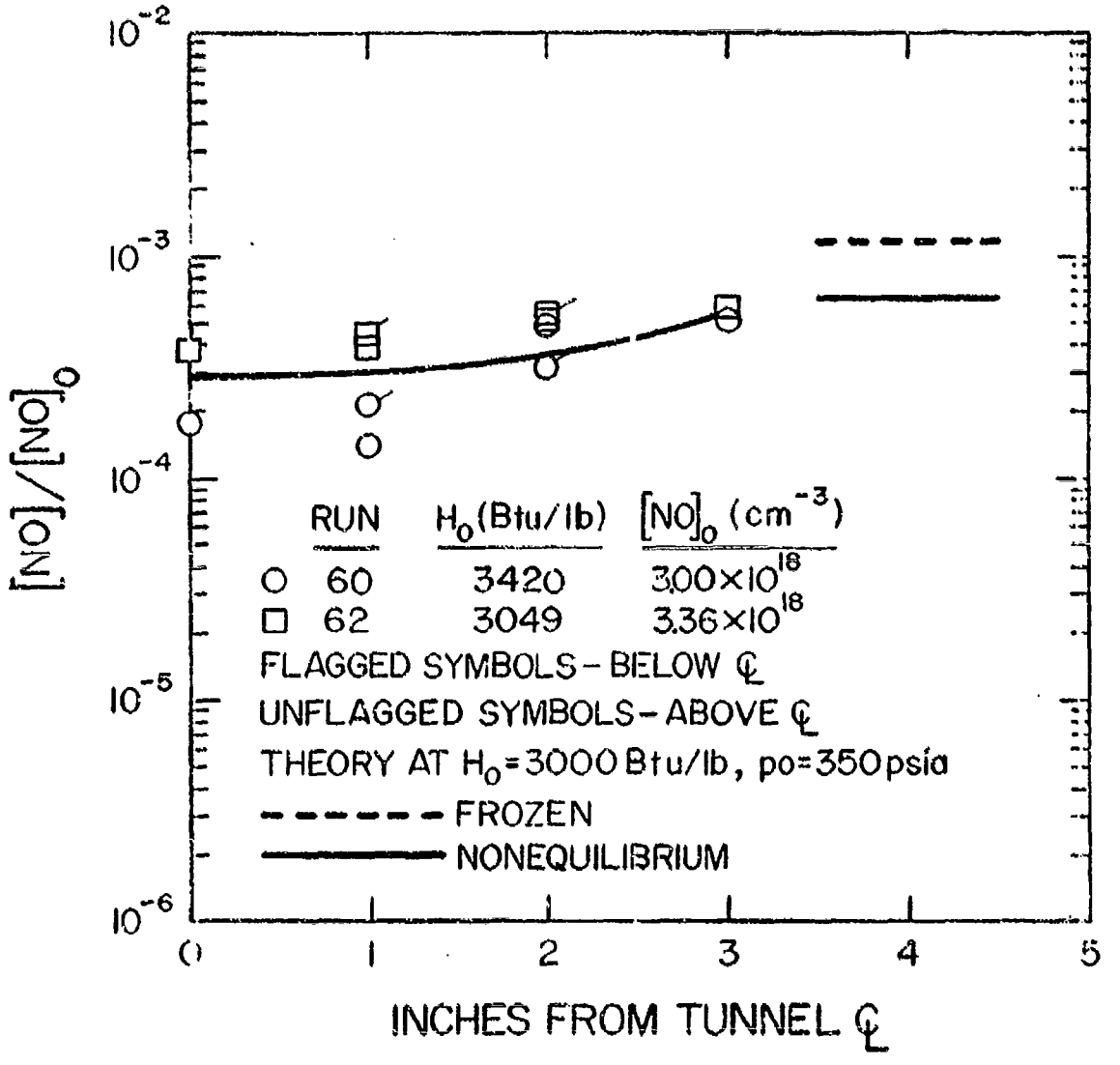

Figure 27. NO Number Densities at Run Condition 2; p_0 = 350 psia; 7-Inch Nozzle

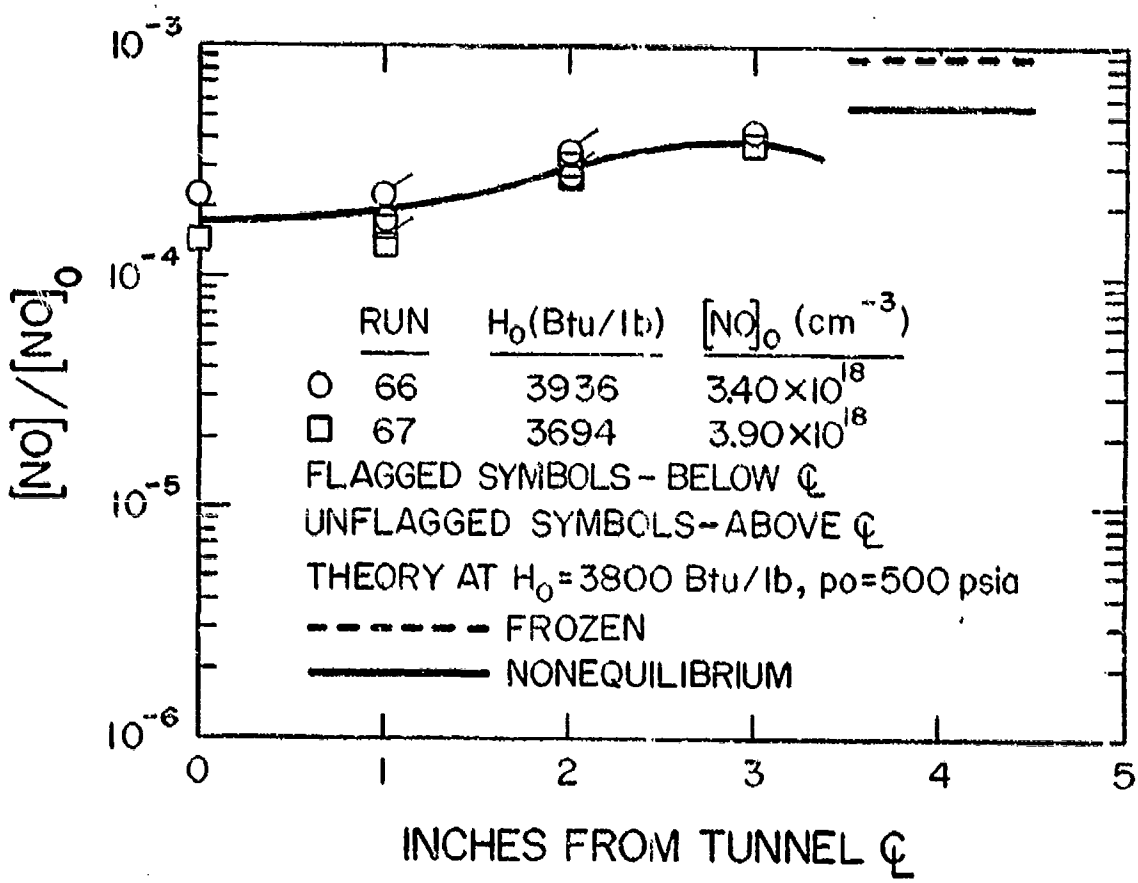

Figure 28. NO Number Densities at Run Condition 3; p_o = 500 psia; 7-Inch Nozzle

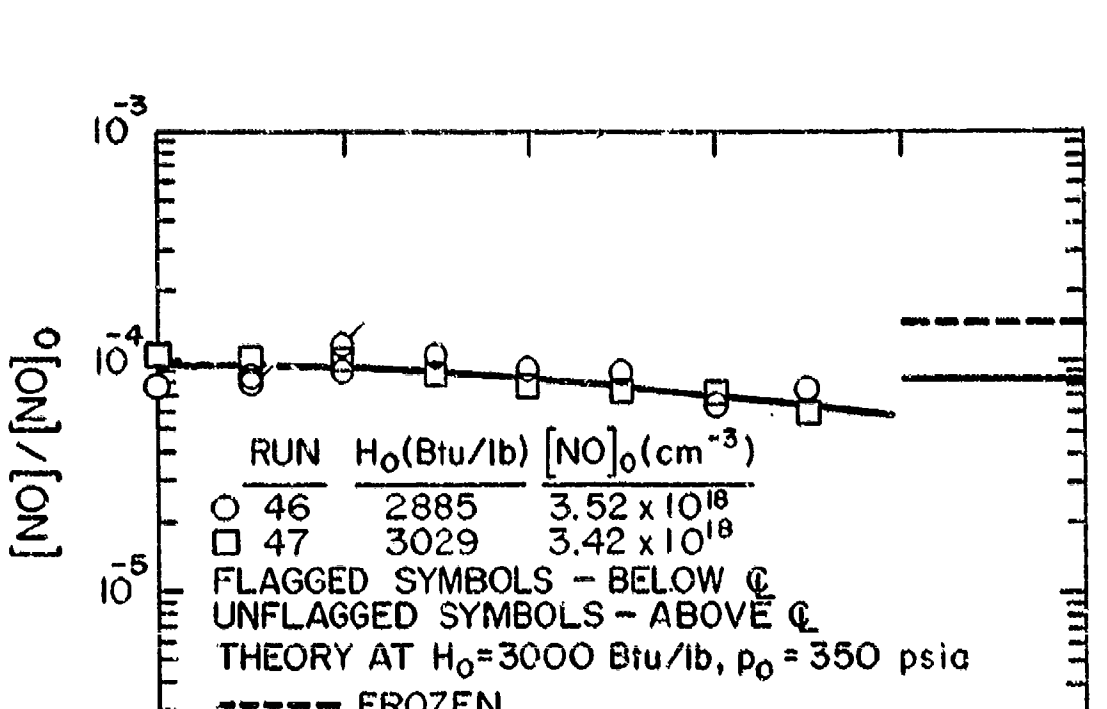

Figure 29. NO Number Densities at Run Condition 2; p_0 = 350 psia; 19-Inch Nozzle

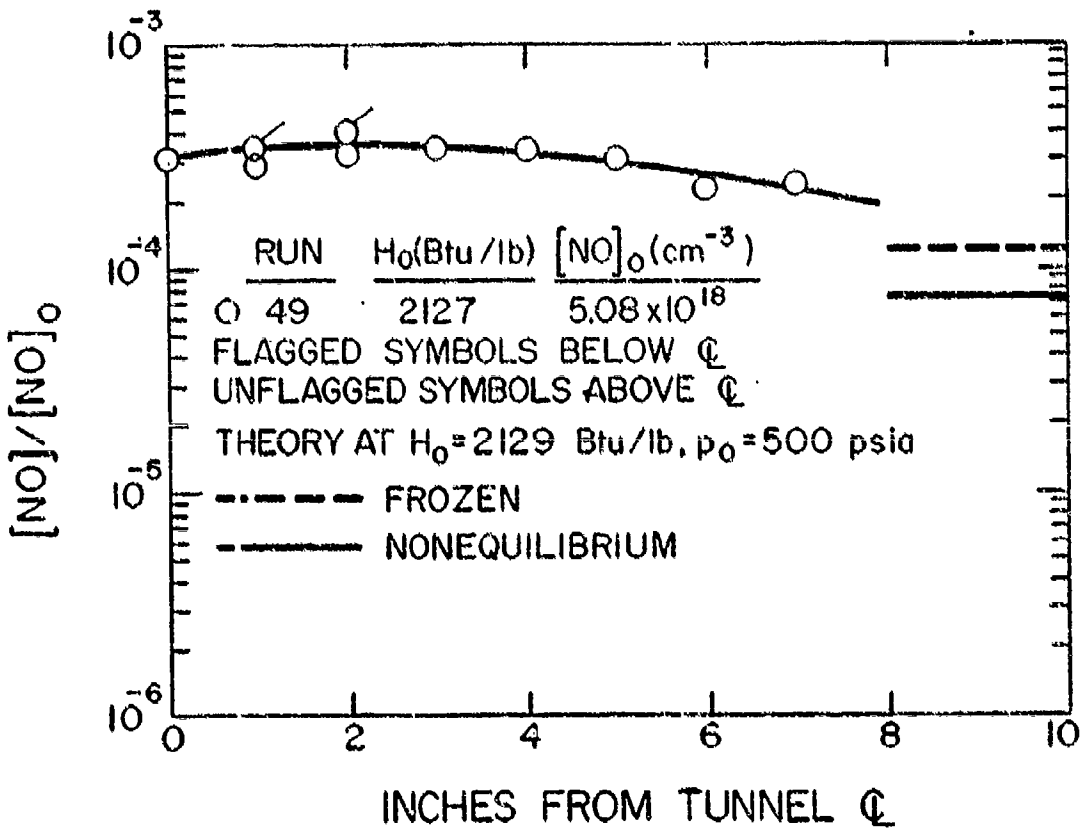

Figure 30. NO Number Densities at Run Condition 3; p_o = 500 psia; 19-Inch Nozzle

suggests that the reaction rates of one or more of the nitric oxide shuffle reactions should be changed to give an increase in the rate of disappearance of nitric oxide. Numerical experimentation with the non-equilibrium flow computer program is required to establish the appropriate shuffle reaction rates. As discussed in Section I, changes in the shuffle reaction rate constants may have important influences on the theoretical predictions of the overall properties of the test gas at the nozzle exit.

Both the molecular nitrogen and nitric oxide species concentrations measured with the electron beam are influenced by the rate of collision quenching. The quenching densities applied in these studies to relate band intensities to number densities were obtained from room-temperature experiments and no translational and/or vibrational influences were included. The collision quenching of the N_2^+ first negative system at the run conditions for the 7-inch nozzle result in quenching factors, $1 + \Sigma N_i/N_i'$, near 1.5. Hence, collision quenching is an important de-excitation mechanism for the N_2^+ first negative system, and errors in the quenching cross sections could be responsible, in part, for the discrepancies between the theoretical and experimental number densities.

Quenching of the NO γ system is much less severe than it is for the N_2^+ first negative system. For the conditions of the 7-inch nozzle tests, the quenching factor was less than 1.17. Hence, collision quenching of the NO γ radiation was not a particularly important factor in converting band intensities to number density. However, the accuracy of the nitric oxide number density measurements depends directly on the applicability of the excitation model proposed here. The relative importance of excitation by secondary and primary electrons must be determined to obtain accurate nitric oxide number density data. The intensities of the NO γ radiation, as a result of excitation by secondary and primary electrons, were determined from room-temperature experiments, and it is possible that different excitation cross sections exist at elevated translational and vibrational temperatures.

VI. CONCLUSIONS

A. ELECTRON BEAM TECHNIQUES

These studies have substantiated the applicability of the high voltage version of the electron beam generator for the 2-Foot Electrogasdynamics Facility. In addition, the applicability of the diagnostic techniques for the measurement of the vibrational temperature and species concentrations of nitric oxide have been demonstrated. Operation of the beam generator at high voltages (40 kV) leads to an increase in the spatial resolution in the measurements because of the associated decrease in elastic scattering of beam electrons. The performance of the beam generator during these tests indicates that it could easily be used at flow densities greater than that corresponding to pressure of 10 Torr at a temperature of 300 K.

The uncertainties associated with the excitation-emission processes for N_2, O, O_2, and NO at high gas densities should be investigated in detail. The relative influences of excitation by secondary and primary electrons should be examined under controlled conditions of elevated translational and vibrational temperatures. The appropriate quenching cross sections for these species must also be known as functions of translational temperature, vibrational temperature, and number density before accurate electron beam data can be obtained at high densities.

Determination of the upper density limit for application of the electron beam technique is required before the full potential of the technique can be realized. From a mechanical point of view, no particular difficulties in generating electron beams suitable for higher density flows are anticipated with the present beam generator configuration.

B. THEORETICAL-EXPERIMENTAL COMPARISONS

The discrepancies between the theoretical and experimental nitrogen number densities experienced in these studies were not expected. It is unlikely that they result from deficiencies in the nonequilibrium theory since the chemical activity of molecular nitrogen in these studies is quite low. The discrepancies probably result from a combination of facility-related effects and unknown errors in the collision quenching cross sections needed to convert band intensities to number density.

Comparisons between the theoretical and experimental nitric oxide number densities indicate that the theory under-predicts the rate of disappearance of nitric oxide within the nozzle expansion process. Numerical experiments with the nonequilibrium flow computer program are required to establish shuffle reaction rates which lead to better agreement between the theoretical and experimental results.

Additional experimental studies should be conducted to obtain temperature and concentration data at enthalpy levels intermediate between those of run condition 1 and run conditions 2 and 3. The results of these studies could then be employed effectively with those from the numerical experiments to isolate the apparent recombination rates applicable to the expansion process. In addition, the concentration and vibrational temperature of molecular oxygen and the concentration of atomic oxygen should be determined at high densities to allow a more complete comparison of the theoretical and experimental results. In all cases, these studies should be performed with the intent of developing a theoretical model for the expansion process which is useful for predicting tunnel calibration data that cannot be measured directly.

REFERENCES

1. Petrie, S. L., Boiarski, A. A. and Lee, H. F., "Electron Beam Flow Field Analyses in the AFFDL Two-Foot Electrogasdynamic Facility," AFFDL-TR-71-161 (1971).

2. Petrie, S. L. and Komar, J. J., "Electron Beam Analysis of the Properties of Molecular and Atomic Oxygen in the AFFDL 2-Foot Electrogasdynamics Facility," AFFDL-TR-73-10 (1973).

3. Petrie, S. L. and Komar, J. J., "Application of the Electron Beam Fluorescence Technique to the Measurement of the Properties of Nitric Oxide in Nonequilibrium Flows," AFFDL-TR-72-144 (1972).

4. Muntz, E. P., "The Electron Beam Fluorescence Technique," AGARD-graph 132, (Dec. 1968).

5. Petrie, S. L., Pierce, G. A. and Fishburne, E. S., "Analysis of the Thermochemical State of an Expanded Air Plasma," U. S. Air Force Flight Dynamics Laboratory Rept. AFFDL-TR-64-191 (1965).

6. Petrie, S. L., "Flow Field Analyses in a Low Density Arc-Heated Wind Tunnel," Proceedings of the 1965 Heat Transfer and Fluid Mechanics Institute, Stanford Univ. Press. (1965).

7. Sebacher, D. I. and Duckett, R. J., "A Spectrographic Analysis of a 1-Foot Hypersonic-Arc-Tunnel Airstream Using an Electron Beam Probe," NASA TR R-114 (1964).

8. Petrie, S. L., et al. "Electron Beam Studies of the Properties of Molecular and Atomic Oxygen," AFFDL-TR-71-30 (1971).

9. Pearse, R. W. B., and Gaydon, A. G., The Identification of Molecular Spectra, Chapmann and Hall Ltd., London (1963).

10. Parobek, D. M., "Performance of Freestream Flow Instrumentation for 9-Inch Contoured Nozzle Tests in the RTD 4-Megawatt Electrogasdynamic Facility," U. S. Air Force Flight Dynamics Laboratory Rept. AFFDL-TR-65-179 (1965).

11. Melton, L. A. and Klemperer, W., Planet. Space Sci. 20, 157 (1972).

12. Mastrup, F. N. and Herrett, R. H., "Optical Scattering Diagnostic Techniques for Hypersonic Arc Flows," AFFDL-TR-71-41 (1971).